Advanced Data Assimilation in Strongly Nonlinear Dynamical Systems*

ROBERT N. MILLER

College of Oceanic and Atmospheric Sciences, Oregon State University, Corvallis, Oregon

MICHAEL GHIL

Department of Atmospheric Sciences and Institute of Geophysics and Planetary Physics, University of California, Los Angeles, Los Angeles, California

FRANÇOIS GAUTHIEZ

Ecole Polytechnique, Palaiseau, France

(Manuscript received 30 December 1991, in final form 15 April 1993)

ABSTRACT

Advanced data assimilation methods are applied to simple but highly nonlinear problems. The dynamical systems studied here are the stochastically forced double well and the Lorenz model. In both systems, linear approximation of the dynamics about the critical points near which regime transitions occur is not always sufficient to track their occurrence or nonoccurrence.

Straightforward application of the extended Kalman filter yields mixed results. The ability of the extended Kalman filter to track transitions of the double-well system from one stable critical point to the other depends on the frequency and accuracy of the observations relative to the mean-square amplitude of the stochastic forcing. The ability of the filter to track the chaotic trajectories of the Lorenz model is limited to short times, as is the ability of strong-constraint variational methods. Examples are given to illustrate the difficulties involved, and qualitative explanations for these difficulties are provided.

Three generalizations of the extended Kalman filter are described. The first is based on inspection of the innovation sequence, that is, the successive differences between observations and forecasts; it works very well for the double-well problem. The second, an extension to fourth-order moments, yields excellent results for the Lorenz model but will be unwieldy when applied to models with high-dimensional state spaces. A third, more practical method—based on an empirical statistical model derived from a Monte Carlo simulation—is formulated, and shown to work very well.

Weak-constraint methods can be made to perform satisfactorily in the context of these simple models, but such methods do not seem to generalize easily to practical models of the atmosphere and ocean. In particular, it is shown that the equations derived in the weak variational formulation are difficult to solve conveniently for large systems.

1. Introduction and motivation

The purpose of this study is to investigate the behavior of advanced data assimilation methods in the context of simple highly nonlinear systems that exhibit such characteristic nonlinear behavior as bifurcation and chaos. The advanced methods implemented are four versions of the extended Kalman filter (EKF) and several variational methods. Ultimately, we expect to use the experience gained from the simple models to guide the application of these advanced techniques to practical problems in data assimilation for the atmosphere and ocean. We focus therefore on the qualitative nature of data assimilation in nonlinear problems rather than on the attributes of any one model or scheme.

Nonlinear systems exhibit a wide variety of behavior types. Here we concentrate on two closely related, intrinsically nonlinear phenomena: bimodality and chaos. Stochastic multimodality arises in systems that exhibit multiple equilibria deterministically. Some systems with multiple equilibria are observed to change abruptly from one equilibrium state to another as the parameters change. This type of behavior is associated with bifurcation. One standard example of bifurcation in solid mechanics is the buckling of an elastic beam.

* Preliminary results of this investigation were presented at the International Symposium on the Assimilation of Observations in Meteorology and Oceanography, Clermont-Ferrand, July 1990, by Miller and Ghil, and at the Assembly of the International Union of Geodesy and Geophysics, Vienna, August 1991.

Corresponding author address: Dr. Robert N. Miller, College of Oceanic and Atmospheric Sciences, Oregon State University, Oceanography Admin. Bldg. 104, Corvallis, OR 97331-5503.

When a beam is compressed along its length, linear theory predicts that the beam will shorten under compression, according to Hooke's law. The linear theory fails when the force of compression becomes so great that the beam buckles. Such bifurcation phenomena are widely known and studied in the physical and biological sciences (May 1973; Rinzel and Miller 1980; Masuda 1982; Guckenheimer and Holmes 1983; Chao 1984; Ghil and Childress 1987).

Chaos is the term used to describe the apparently random behavior exhibited by certain deterministic dynamical systems. The best-known example is the celebrated Lorenz (1963) model, a truncation of the Rayleigh–Bénard equations describing convection. Chaotic behavior, however, is not restricted to models with low-order truncation, but has been shown rigorously to exist in many fluid systems described by the full equations of motion (Témam 1988; Constantin et al. 1989). Chaotic behavior has also been observed in the laboratory for many types of flow (e.g., Libchaber 1985). In this study, we use two qualitative examples which exhibit nonlinear behavior of particular interest, in order to examine the expected performance of data assimilation methods for strongly nonlinear systems.

What do we want from data assimilation methods in the presence of nonlinearity? Our provisional answer is that, in the case of bifurcation, we want our scheme to indicate the correct qualitative state of the system; that is, we do not want the model to tell us that the beam is buckled if it is straight, and vice versa.

In the case of chaotic behavior, our objective is similar in that we want our scheme to indicate the correct quantitative state of the system in the short term, and the correct qualitative state of the system in the long term. We also need reliable error estimates: we do not want the model to tell us that its predictions are reliable when, in fact, they are no better than chance.

Ghil et al. (1981) suggested that, based on experience with highly suboptimal operational data assimilation in meteorology, the EKF should be the method of choice for extending the Kalman filter, known to be optimal for linear systems, to the nonlinear ones encountered in atmospheric and oceanic dynamics. Kushner (1967), however, applied the EKF to the Van der Pol equation and found that the filter became unstable and failed to produce useful estimates of the model state. He modified the EKF to obtain a stable filter by adding an estimate of the fourth moments in terms of the covariances, while the standard EKF is formulated entirely in terms of covariances, that is, second-order moments, and higher-order quantities are neglected. In Kushner's example the data consisted of very sparse measurements of only one of the state variables, and the measurement error had a standard deviation the same size as the total amplitude of the periodic motion.

While Kushner's (1967) results prompt us to approach the problem with some caution, extensive experience with the EKF in the engineering literature (e.g., Gelb 1974) indicates that it works quite well under less extreme conditions. In particular, Budgell (1986) in oceanography and Lacarra and Talagrand (1988) in meteorology have shown that the successive linearizations, which form the basis of the EKF, work well when advective nonlinearity is not combined with strong instability. We study here the performance of the EKF along with an extension through third and fourth moments, and an empirical simplification of the latter using Monte Carlo simulation.

A number of investigators have applied variational formulations to nonlinear problems in meteorology (Sasaki 1958) and oceanography (Provost and Salmon 1986). In these methods, one defines some measure of total error, usually referred to as a "cost function" or "objective function," and estimates the values of the control parameters, which minimize the total error in this sense. As a simple example, the cost function might be the mean-square difference between the model solution and observed data, and the parameters might be the initial values on a finite-difference grid for the model. In most practical problems, the dimension of the space of control parameters is so large as to make Newton-type methods unfeasible; hence descent methods are used, typically conjugate gradient methods. The gradient of the cost function is calculated by solving an adjoint problem; this can be readily derived by the standard formalism of the calculus of variations. For this reason, such methods are sometimes known as "adjoint methods."

In recent years, a number of adjoint methods have been applied to prototype problems in numerical weather prediction (e.g., Courtier and Talagrand 1987; Derber 1989). More recently Gauthier (1992), in a study similar to the present one, applied an adjoint method to the Lorenz model and used the results for guidance in analysis of an adjoint calculation with a nondivergent barotropic model on the sphere. Such methods have also been proposed for diagnostic analysis of the mean ocean circulation by Schröter and Wunsch (1986) and by Tziperman and Thacker (1989). These methods are appealing in that they are conceptually simple and potentially economical in terms of computing resources and they use all of the available data in a natural way. Error estimates for the control parameters can be calculated using the Hessian of the cost function with respect to these parameters (e.g., Tziperman and Thacker 1989), but this is a resource-intensive calculation, comparable in effort to computation of error covariances in the Kalman filter. Detailed error estimates for the complete analyzed fields are hard to come by in this framework, while they are a natural by-product of the EKF.

There is a well-known underlying duality between variational inverse calculations and the Kalman filter (Bennett and Budgell 1989 and references therein; Gaspar and Wunsch 1989; Ghil and Malanotte-Rizzoli 1991, section 5.4.1 and Table 4). One may calculate

the solution of the variational problem by the Kalman smoother, an augmented form of the Kalman filter in which all of the data in the time interval of interest are taken into account. As in the Kalman filter, error covariance estimates are calculated. This calculation can be extremely costly; the variational methods owe much of their economic advantage precisely to the fact that one can avoid it. We investigate several variational techniques in detail in the present work and compare them to the EKF and to other extensions of the Kalman filter for nonlinear problems.

In this study, we apply advanced data assimilation techniques to two simple systems of nonlinear ordinary differential equations (ODEs): the stochastically forced double-well model and the aforementioned Lorenz model. A derivation of the extended Kalman filter is presented in section 2. Results of data assimilation experiments with the double-well system are described in section 3. Results for the Lorenz system are given in section 4. Section 5 contains a brief summary and discussion of results. Details of the numerical methods used to calculate solutions of stochastic differential equations are given in appendix A, and a discussion of the statistical characteristics of trajectories of the Lorenz model appears in appendix B.

2. The extended Kalman filter (EKF): Derivation and basic assumptions

Statistically optimal analysis methods for nonlinear systems involve, theoretically, an infinite number of equations for the moments. This is formally identical to the closure problem in turbulence theory, and can be illustrated by a simple formal calculation. Begin with the ODE:

$$\dot{x} = f(x)$$

and try to estimate the expected value $\hat{x}$ of x; we shall also use $E(\ )$ to denote expected value. We have $\hat{\dot{x}} = \widehat{f(x)} \neq f(\hat{x})$ unless f is linear.

The easiest thing to do is expand f in a Taylor series:

$$f(x) = f(\hat{x}) + (x - \hat{x})f'(\hat{x}) + (1/2)(x - \hat{x})^2 f''(\hat{x}) + \cdots.$$

Thus,

$$\begin{aligned}\widehat{f(x)} &= f(\hat{x}) + \widehat{(x - \hat{x})}f'(\hat{x}) + (1/2)\widehat{(x - \hat{x})^2}f''(\hat{x}) + \cdots \\ &= f(\hat{x}) + (1/2)Pf''(\hat{x}) + (1/6)\widehat{(x - \hat{x})^{33}}f'''(\hat{x}) + (1/24)\widehat{(x - \hat{x})^4}f''''(\hat{x}) + \cdots,\end{aligned}$$

where $P = \widehat{(x - \hat{x})^2}$ is the variance or centered second moment. We may write an equation for P:

$$\begin{aligned}\dot{P} \equiv \dot{\widehat{(x - \hat{x})^2}} &= 2\widehat{(x - \hat{x})}f(\hat{x}) + 2Pf'(\hat{x}) + \widehat{(x - \hat{x})^3}f''(\hat{x}) + (1/3)\widehat{(x - \hat{x})^4}f'''(\hat{x}) + \cdots \\ &= 2Pf'(\hat{x}) + \widehat{(x - \hat{x})^3}f''(\hat{x}) + (1/3)\widehat{(x - \hat{x})^4}f''' + \cdots.\end{aligned}$$

The expression for the evolution of the second-order moment involves therewith the third moment, and so on. The extended Kalman filter (EKF) can be easily derived in the discrete form in which it is actually implemented. Assume that the evolution of the underlying natural system is given, following the notation of Ghil et al. (1982), by

$$x^t_{k+1} = f(x^t_k) + \sigma b_{k+1}, \tag{2.1a}$$

while the model system is given by

$$x^f_{k+1} = f(x^a_k); \tag{2.1b}$$

the superscripts t, f, and a denote "truth," "forecast," and "analysis," respectively, subscripts denote time step, and b_j is a Gaussian white sequence with unit variance. By "analysis," we mean our best estimate of the state variable at an observation time.

We can find an expression for the evolution of the error variance P corresponding to the discrete form of the stochastic differential equation described above. The evolution of the error itself is given by

$$\begin{aligned}x^t_{k+1} - x^f_{k+1} &= f(x^t_k) - f(x^a_k) + \sigma b_{k+1} \\ &= (x^t_k - x^a_k)f'(x^a_k) + \frac{1}{2}(x^t_k - x^a_k)^2 f'' + \frac{1}{6}(x^t_k - x^a_k)^3 f'''(x^a_k) + \frac{1}{24}(x^t_k - x^a_k)^4 f''''(x^a_k) + \cdots + \sigma b_{k+1}.\end{aligned} \tag{2.2}$$

Squaring and taking expected values leads to

$$\begin{aligned}P^f_{k+1} &\equiv E[(x^t_{k+1} - x^f_{k+1})^2] \\ &= E[(x^t_k - x^a_k)^2](f'(x^a_k))^2 + E[(x^t_k - x^a_k)^3]\{[f'(x^a_k)]^3 + f'(x^a_k)f''(x^a_k) \\ &\quad + E[(x^t_k - x^a_k)^4] \times \left(\frac{1}{4}(f''(x^a_k))^2 + \frac{1}{3}f'(x^a_k)f'''(x^a_k)\right) + \cdots + \sigma^2.\end{aligned} \tag{2.3}$$

The simplest way to close (2.3) is to discard moments of third and higher order. This approach yields

$$P^f_{k+1} = E[(x^t_k - x^a_k)^2](f'(x^a_k))^2 + \sigma^2$$
$$\equiv P^a_k(f'(x^a_k))^2 + \sigma^2. \quad (2.4)$$

If there is an observation x^o_{k+1} at time step $k+1$, the *innovation* $x^o_{k+1} - x^f_{k+1}$ may be combined with the forecast state x^f_{k+1} to form the analysis x^a_{k+1} by the formula

$$x^a_{k+1} = x^f_{k+1} + K_{k+1}(x^o_{k+1} - x^f_{k+1}), \quad (2.5)$$

where K_{k+1} is the Kalman gain, given by

$$K_{k+1} = P^f_{k+1}/(P^f_{k+1} + R), \quad (2.6)$$

and R is the observation error variance. The analysis error variance is given by

$$P^a_{k+1} = (1 - K_{k+1})P^f_{k+1}. \quad (2.7)$$

Formulas (2.1) and (2.4) through (2.7) define the EKF for a scalar system. Generalization to vector systems is straightforward (cf. Jazwinski 1970). The prediction is given by

$$\mathbf{x}^f_{k+1} = \mathbf{f}(\mathbf{x}^a_k), \quad (2.8a)$$

where $\mathbf{x}$ is the state vector and $\mathbf{f}$ is the nonlinear function that defines the state evolution. The covariance evolution is given by

$$\mathbf{P}^f_{k+1} = [D\mathbf{f}]\mathbf{P}^a_k[D\mathbf{f}]^{\mathrm{T}} + \mathbf{Q}, \quad (2.8b)$$

where $\mathbf{P}^{f,a}_k$ is the model-forecast (analysis) error-covariance matrix, $\mathbf{Q}$ is the system-noise covariance matrix, and $D\mathbf{f}$ is the matrix of partial derivatives of $\mathbf{f}$ evaluated at the current analysis point $\mathbf{x}^a_k$. The observation process is described by

$$\mathbf{x}^o_{k+1} = \mathbf{H}\mathbf{x}^t_{k+1} + \mathbf{b}^o_{k+1}, \quad (2.8c)$$

where $\mathbf{x}^o_{k+1}$ is the vector of observations at time t_{k+1}, $\mathbf{H}$ is the matrix that relates the true state vector $\mathbf{x}^t_{k+1}$ to the observation vector $\mathbf{x}^o_{k+1}$, and $\mathbf{b}^o_{k+1}$ denotes the observation noise. We could relax the assumption that the measurement functional is linear, at the cost of a slight increase in complication.

The update is given by

$$\mathbf{x}^a_{k+1} = \mathbf{x}^f_{k+1} + \mathbf{K}_{k+1}(\mathbf{x}^o_{k+1} - \mathbf{H}\mathbf{x}^f_{k+1}) \quad (2.8d)$$

and the Kalman gain matrix $\mathbf{K}_{k+1}$ by

$$\mathbf{K}_{k+1} = \mathbf{P}^f_{k+1}\mathbf{H}^{\mathrm{T}}(\mathbf{H}\mathbf{P}^f_{k+1}\mathbf{H}^{\mathrm{T}} + \mathbf{R})^{-1}, \quad (2.8e)$$

where $\mathbf{R}$ is the observation noise covariance matrix. The error covariance of the updated state vector is given by

$$\mathbf{P}^a_{k+1} = (\mathbf{I} - \mathbf{K}_{k+1}\mathbf{H})\mathbf{P}^f_{k+1}. \quad (2.8f)$$

3. The double-well potential

a. Overview

The double-well model is a stochastically forced nonlinear scalar ODE with equilibria at 0, 1, and -1. Of these, 0 is unstable and 1 and -1 are stable in the absence of stochastic forcing. When weak stochastic forcing is applied, the system will stay near one of the stable equilibria most of the time. Occasionally, however, a sequence of perturbations will occur that forces the system to the other stable equilibrium; this is what is meant by a transition in such a system. This is not a bifurcation in the same sense as the buckling of a beam, but it allows a first test of the ability of the EKF to follow state transitions. Weak stochastic forcing is the conceptual counterpart, in this simple model, of subgrid-scale noise in a realistic model of the ocean or atmosphere. Systems of this form have been proposed as models of terrestrial climate in which the two equilibria represent conditions like the present ("normal conditions") and ice ages (Nicolis and Nicolis 1981; Sutera 1981).

The underlying deterministic dynamics are given by the following simple nonlinear scalar system:

$$\dot{x} = f(x) \equiv -4x(x^2 - 1). \quad (3.1)$$

This can be viewed as a system whose dynamics are given by the negative gradient of the potential function $F(x) = x^2(x^2 - 2)$.

From this point of view, wells appear at $x = 1$ and $x = -1$ while a relative maximum occurs at $x = 0$. Any solution of this equation that does not have its initial value exactly equal to zero will tend to one of the two stable equilibria. If stochastic forcing is applied, the resulting stochastic differential equation is

$$dx = f(x)dt + \sigma db, \quad (3.1')$$

where b is a Wiener process whose increments have unit variance. Eventually, the random process will generate a long enough series of increments with the same sign that the system will move from the basin of attraction of one equilibrium state to that of the other. An asymptotic formula due to Kramers (1940) for the mean residence time $\hat{\theta}$ in each well is given by

$$\hat{\theta} \approx \frac{\pi}{[-F''(0)F''(1)]^{1/2}} \exp\left[\frac{F(0) - F(1)}{\sigma^2/2}\right],$$

for $\sigma \ll F(0) - F(1)$.

To make meaningful comparisons with the existing theory of transitions between the two "states" of a double-well model, we must first determine what we mean by a state transition. Naively, one would think that a transition takes place when two successive states take on different signs, but this is not satisfactory because $x = 0$ is a fixed point of the system (albeit an unstable one), so the trajectory of the system will often remain in the vicinity of $x = 0$ for a while, taking on both signs, before falling definitely into one basin or another. We expect from experience that the boundary layer, which forms about $x = 0$, will have width proportional to σ (Schuss 1980).

We chose $\sigma^2 = 0.24$ in (3.1′) and used the trapezoidal rule (see appendix A) to integrate it. In numerical experiments with integration times up to 100 000, Kramers's formula does not give a reliable estimate of $\hat{\theta}$. Ultimately, for sufficiently small σ, Kramers's formula would be reliable, but the time between state transitions would then be extremely long [see discussion of these difficulties and further references in Ghil and Childress (1987), pp. 324–328 and 350–351].

b. *The extended Kalman filter*

1) Effectiveness in different parameter ranges

As long as the state variable remained in one well or the other, the EKF functioned reliably, producing accurate estimates of the state and the error variance, for all reasonable parameter choices. The ability of the system to track transitions of the state from one well to the other varied with the accuracy and frequency of observations. Results of three experiments with different outcomes are shown in Fig. 1.

In the run depicted in Fig. 1a, the filter tracked the true system reliably, producing a state transition as soon as observations sensed it. In Fig. 1b, a case with less accurate observations, the filter failed to track the state transition. Corrections in the right direction were produced, but they were of insufficient magnitude to force a transition. In the run depicted in Fig. 1c, with the same observational error as in 1b but with more frequent observations, the filter did produce the correct state transition; it did so even sooner than in Fig. 1a, due to the shorter update interval. In both Figs. 1a and 1c, the estimated state lagged the true state by a single observational interval.

The time scale of the dynamics determined by linearizing the system about one of the stable equilibria is 0.125 near the equilibrium. The results in Fig. 1a show that we can sample much less frequently than that and still get reliable filter performance.

In the failure mode observed in Fig. 1b, we shall see that the model can (almost) never be expected to produce a transition. More frequent sampling will fix the problem, as shown in Fig. 1c. More accurate measurements will also fix the problem. These results can be explained by a simple qualitative argument.

2) Qualitative explanation and semianalytical results

If the measurements are perfect ($R = 0$), the system will be reinitialized every observation, and the transitions in the estimated state will lag those in the true state by at most one sampling interval. In the case of perfect measurements, the filter gain is unity [cf. Eq. (2.6)]. In fact, if the observations are accurate enough to make the filter gain greater than 0.5, then the filtered output will track the transitions of the true system,

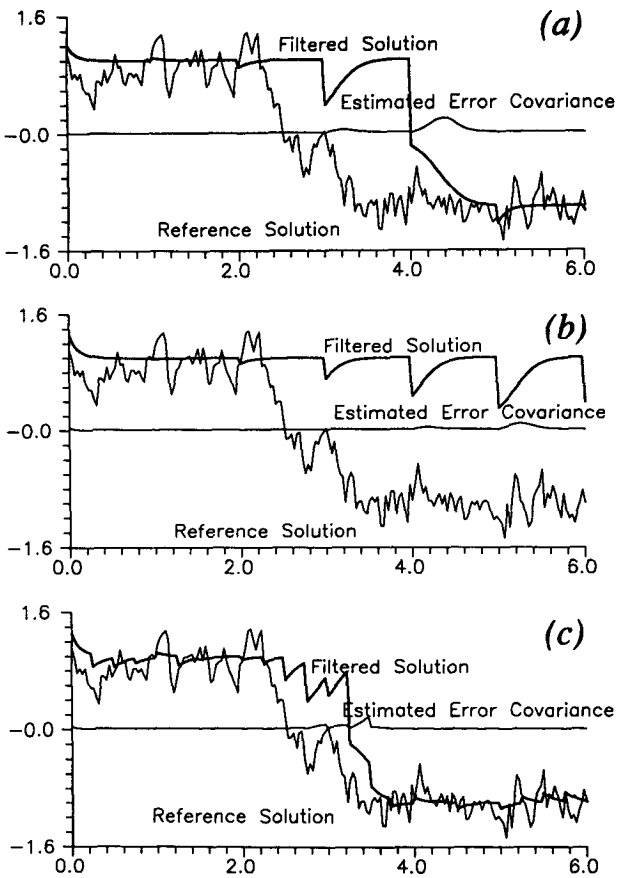

FIG. 1. Results of applying the extended Kalman filter (EKF) to the double-well problem. Stochastic perturbation term has variance 0.24. (a) Variance of observation errors is $R = 0.01$; observations are taken at intervals of 1.0 time units. (b) $R = 0.04$; observations at intervals of 1.0. (c) $R = 0.04$; observations taken at intervals of 0.25.

again lagged by at most one sampling interval. The reason for this is simple: if the modeled and true systems are in different basins, a gain greater than 0.5 will usually move the model system into the other basin. This case is shown in Fig. 1a.

If the sampling interval is very long compared to the typical time scale of the dynamics, then the model system and its associated error variance will relax almost all the way to equilibrium between observations. In that case, it is easy to derive upper bounds on system measurement errors sufficient to make the model track the true system. At equilibrium, say $x = 1$, the forecast error variance P approaches a steady value of $P_\infty \equiv \Delta t\sigma^2/[1 - (1 - 8\Delta t)^2] \approx \sigma^2/16$.

Thus, if sampling is too infrequent, $x \approx \pm 1$ and $P \approx P_\infty$ over the latter part of the interval between samples. If the observation error variance R is greater than or equal to P_∞, then examination of Eqs. (2.5) and (2.6) shows that updating will not force the model into the other state. This is the case demonstrated in Fig.

1b. The estimated model-error covariance is so small that there is not enough gain to force a transition from the positive to the negative basin, or vice versa. More accurate measurements will fix the problem, as seen before.

Less accurate measurements can be tolerated if the sampling interval is decreased. In the case in which the filter gain is insufficient to move the system from one basin to the other, two successive updates with data from the other basin may be sufficient. This is the case shown in Fig. 1c. In that case, four updates were required to force the model from the positive to the negative basin. This is the "nudged" case. Because the estimated error variance P does not have time to relax to P_∞ between updates, subsequent updates are given greater weight, so the covariance, and therefore the filter gain, is modified further, along with the state variable.

c. *Variational methods*

The simplest of the variational methods, termed the "strong constraint method" by Sasaki (1970), in which the result is an exact solution of the dynamical model, cannot be applied here. A strong-constraint scheme will not produce a state transition, since no state transition can occur in the solution of the deterministic dynamical model (3.1). Weak-constraint methods, in which the cost function is some positive-definite function of the model residuals and the differences between the data and the model predictions, are more difficult to implement, since the output of the scheme is no longer determined uniquely by initial (and, in general, boundary) conditions. Here we follow the approach of Bennett and Budgell (1989), generalized to nonlinear problems.

A suitable cost function for this problem is

$$J(x) = \frac{1}{2\sigma^2}\int_{t_0}^{T} [\dot{x} - f(x)]^2 dt + \frac{\Delta T}{2R}\sum_{j=0}^{N-1} [x(t_j) - x_j]^2,$$

where $f(x)$ is as in (3.1), T is the final time, ΔT is the interval between observations, t_j are the observation times, x_j are the observations, and $T - t_0 = N\Delta T$. We assume for convenience that $t_0 = 0$. It is a simple exercise in the calculus of variations (e.g., Courant and Hilbert 1953) to show that the corresponding Euler–Lagrange equations are given by

$$\dot{\lambda} + f'(x)\lambda = \frac{\Delta T}{R}\sum_{j=1}^{N-1} [x(t_j) - x_j]\delta(t - t_j), \quad (3.2a)$$

$$\lambda(T) = 0, \quad (3.2b)$$

$$\lambda(0) = \frac{\Delta T}{R}(x(0) - x_0), \quad (3.2c)$$

$$\dot{x} - f(x) = \sigma^2\lambda, \quad (3.2d)$$

where $\delta(s)$ is the Dirac delta function, and the adjoint variable λ is defined by (3.2d).

This set of equations is difficult to solve in highly nonlinear cases such as the double-well problem. The simplest functional iteration scheme would proceed by using the current guess for x to compute the adjoint variable λ by integrating (3.2a) backwards in time, subject to final conditions (3.2b), which would, in turn, be used to compute the new x by integrating (3.2d) forward in time subject to (3.2c). It is easy to see that this scheme must fail, since a good guess for x would result in small innovations, and thus small values of λ. This would yield in turn weak forcing in the original equation for x, which would then result in a new estimate with no state transition. Straightforward transformations of x and linearizations of f about one of the stable equilibria also fail.

Newton's method and generalizations such as quasilinearization (e.g., Bryson and Ho 1975, chapter 7) lead to practical computational problems of a sort we wish to avoid. To illustrate these problems, consider Newton's method for the Euler–Lagrange equations (3.2a–d). This method can be derived in the following way. Suppose the pair of functions (x, λ) is a good estimate of the solution to (3.2a–d). Then the exact solution can be written as $(x + \Delta x, \lambda + \Delta\lambda)$ where Δx and $\Delta\lambda$ are small. Substituting $x + \Delta x$ and $\lambda + \Delta\lambda$ for x and λ in (3.2a–d) and discarding quadratic and higher-order terms yields

$$\dot{\Delta\lambda} + f'(x)\Delta\lambda + f''(x)\lambda\Delta x - \frac{\Delta T}{R}\sum_{1}^{N-1} \Delta x(t_j)\delta(t - t_j) = \rho_\lambda, \quad (3.3a)$$

$$\Delta\lambda(T) = 0, \quad (3.3b)$$

$$\Delta\lambda(0) = \frac{\Delta T}{R}\Delta x(0), \quad (3.3c)$$

$$\dot{\Delta x} - f'(x)\Delta x - \sigma^2\Delta\lambda = \rho_x, \quad (3.3d)$$

where ρ_λ and ρ_x are the residuals from the equations for λ and x in (3.2a) and (3.2d) at the current guess. The problem is that—unlike the more familiar case of the adjoint equations in the strong-constraint approach—the $\Delta\lambda$ and Δx equations are coupled, and one cannot integrate them separately. In the strong-constraint approach (e.g., Le Dimet and Talagrand 1986), one integrates the adjoint equation (3.3a) backwards in time, followed by a forward integration of (3.3d); both of these integrations are stable. The Δx term in (3.3a) defeats that strategy here.

One could devise an iteration scheme in which one placed the $f''(x)\lambda\Delta x$ term in (3.3a) on the right-hand side and evaluated it at the current iterate; this would be the functional equivalent of the familiar Gauss–Seidel scheme of numerical linear algebra. Unfortunately, the theorems that set forth conditions for convergence of the Gauss–Seidel scheme involve bounds on the upper triangular component (e.g., Forsythe and Moler

1967); in the present context, these bounds imply that the scheme will work only for weakly nonlinear models.

It is possible to minimize the cost function directly by using numerical quadrature to approximate the integral and differentiating the quadrature formula to calculate the gradient of the cost function with respect to the discrete values of x. Less than 200 values of x were calculated in the runs from which Fig. 1 was generated, and standard optimization algorithms such as the conjugate gradient method can be used. This brute force tactic is impractical for problems which involve realistic atmospheric or oceanic models [but see Ghil and Malanotte-Rizzoli (1991), section 5.4.2 and references]. We perform the direct calculation here for completeness and, more important, to gain experience with the behavior of approximate solutions to the variational problem.

If the EKF is used to provide the initial guess for the optimization algorithm in a case such as that shown in Fig. 1b, it is unlikely that the optimization algorithm will find a solution with a state transition. The IMSL (1989) conjugate gradient routine in fact failed in that case. A modified EKF can be constructed that will follow the state transition in the reference solution, and thus provide an adequate first guess for the weak-constraint method.

Here we follow the approach of Kailath (1968) to the Kalman filter in deriving a modification based on examining the innovation sequence, $(x_k^o - x_k^f)$ or—more generally—$(\mathbf{x}_k^o - \mathbf{H}\mathbf{x}_k^f)$, where $\mathbf{H}$ defines the relation between the state vector and the observed quantities. For a linear system, the sequence

$$[(\mathbf{x}_k^o - \mathbf{x}_k^f), (\mathbf{H}\mathbf{P}_k^f\mathbf{H}^T)^{-1}(\mathbf{x}_k^o - \mathbf{x}_k^f)] \quad (3.4)$$

should be χ^2 distributed, and thus, examination of sequence (3.4) will reveal whether or not the Kalman filter is functioning correctly. Devices such as this—informally known as "sanity checkers"—can be constructed for the EKF. If the sequence fails the χ^2 test, the system can be reinitialized, or the value of σ^2 used in the calculation of the error covariance P can be artificially increased.

A technique based on (3.4) was applied to the case shown in Fig. 1b, that is, the case in which the EKF failed to follow the transitions in the reference solution. The series of observations was too short to perform a χ^2 test; instead, the filtered output was forced into the opposite basin if the average of two successive innovations was greater than 1.1 in absolute value. If that proved to be the case, the system-noise variance was also doubled. Its original value was restored if the average of two successive innovations was less than the root-mean-square observation error.

Figure 2 shows the results of the modified EKF and the variational solution. The cost function was reduced by nearly an order of magnitude from its first-guess value using a conjugate gradient method for direct minimization, but most of the reduction results simply from the greater smoothness of the variational solution. Experiments were performed with a wide range of parameter values, and in no case did the conjugate gradient solver produce a state transition which was not present in the initial guess, provided by the modified EKF.

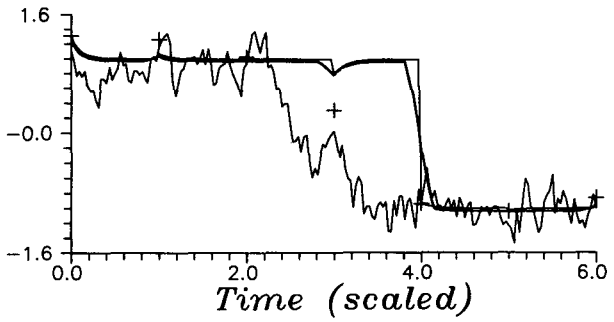

FIG. 2. Solution of the smoothing problem for the double-well model. The variationally smoothed solution is shown as the heavy line. The Kalman-filtered and reference solutions are shown as thin lines; the latter is more jagged and identical to the one shown in Figs. 1a–c. The observations are shown as "+" signs.

4. The Lorenz equations

a. Overview

The system of equations now known as the Lorenz model is a Fourier truncation of the flow equations governing thermal convection. It was introduced by Lorenz (1963) and has generated an entire body of literature of its own; for a review of some of the major work see Sparrow (1982). The Lorenz model was the first system of ODEs shown to possess chaotic solutions, that is, solutions that are apparently random over long times, despite the fact that, as in any system of ODEs defined in terms of smooth functions, solutions are unique and depend smoothly upon initial data over short times. The governing equations are

$$\dot{X} = \sigma(Y - X), \quad (4.1a)$$

$$\dot{Y} = \rho X - Y - XZ, \quad (4.1b)$$

$$\dot{Z} = XY - \beta Z. \quad (4.1c)$$

The parameter values first used by Lorenz to obtain chaotic solutions are $\sigma = 10$, $\rho = 28$, and $\beta = 8/3$, where σ is the Prandtl number, ρ a normalized Rayleigh number, and β a nondimensional wavenumber. These values are still the most common ones, and will be used throughout here.

The system has three equilibrium points: the origin represents the conductive state of no motion, and the two others, at $[\pm\sqrt{\beta(\rho - 1)}, \pm\sqrt{\beta(\rho - 1)}, \rho - 1]$, each represent a pattern of convection rolls, differing by their direction of rotation. All three equilibria are unstable for this choice of parameters. The origin is a saddle with a single unstable mode in the X–Y plane.

The two convective states are unstable spiral points. The eigenvalue associated with the third principal direction of the latter is real and negative.

The system exhibits statistical bimodality due to the solutions looping in phase space around one of the two convective states, then the other, then back around the first, and so on, ad infinitum. The chances for a given loop to occur around one convective state or the other are exactly those of a fair coin coming up heads or tails, in spite of the perfectly deterministic nature of the system. Schematic diagrams of the phase space of the Lorenz equations, showing the stable and unstable manifolds of the fixed points, appear in Ghil and Childress (1987, Figs. 5.10–5.12). Quantitative details of this conceptual picture are given in appendix B.

b. *Application of the EKF*

For the Lorenz equations, we computed a reference solution with initial values (1.508870, −1.531271, 25.46091), and constructed a sequence of "observations" from it, that is, values of the reference solution contaminated by noise, at regular intervals; no stochastic forcing was added to the model. The duration of the experiment was 20 (dimensionless) time units; the oscillations about the convective state take place with roughly unit time scale.

We then attempted to estimate the values of the reference solution by using the EKF to assimilate data into the equations. It is well known that the chaotic character of the behavior of the system is due to the sensitive, albeit smooth, dependence of its solutions on initial data. Hence, only a minute error in the initial data used is necessary to test whether the assimilated data will keep the solution "on track," and prevent divergence from the reference solution. Bimodality here is connected intimately with the exponential instability of solutions, making this test case more realistic with respect to the properties of intense geophysical jets, atmospheric or oceanic, with their barotropic and baroclinic instabilities.

In the EKF, the estimate of the error covariance **P** is not directly influenced by the innovation sequence. The only influence of the sequence of innovation vectors on the evolution of **P** is through their influence on the updated fields, which, in turn, determine the evolution operator. In particular, **P** can be small when the innovation vectors are large.

In weakly unstable systems, such as the Lorenz equations in the vicinity of one of the convective states, the estimate of the solution error covariance generated by the EKF will eventually be much smaller than the observation error covariance (e.g., Ghil et al. 1981; Ghil 1989). Following a period of initial adjustment, the weights assigned to the observations will be very small as long as the estimate of the state vector remains near a convective state. Therefore, the estimated state vector must pass through a region of strong instability if significant corrections are to be made. It is only near the Z axis, particularly in the neighborhood of the saddle at the origin, that the system is strongly unstable. In general, transitional trajectories from one convective state to the other pass near the saddle. If in some small time interval the true system undergoes a transition and the estimated solution does not, as will eventually happen with any pair of trajectories, the true and estimated solutions will be in different basins, but the correction will be small and the estimated solution will remain in the same basin in which it started.

Results of the EKF experiment are shown in Figs. 3 and 4 for the X and Z variables. It is not necessary to show the Y variable, given the reflection symmetry of the Lorenz model in the Z axis. In this experiment, the observation noise was Gaussian with variance equal to 2. Observations were provided at intervals of 0.25. From Fig. 3a, we can see that the EKF tracked the true solution through several loops, underwent a transition

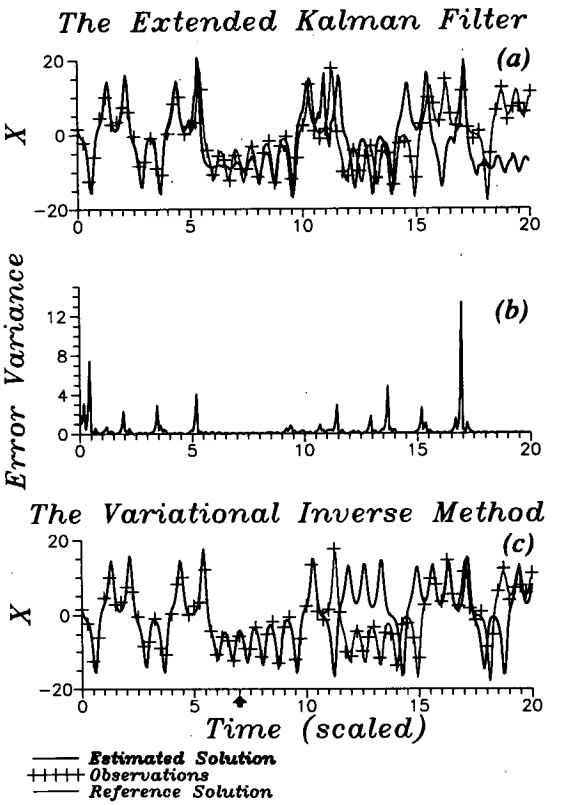

FIG. 3. Results of filtering and smoothing experiments for the Lorenz model. (a) Estimate of the state variable X by the extended Kalman filter (EKF). Thin line: reference solution; plus signs: simulated observations; heavy line: filtered output. (b) Estimated error variance from the EKF corresponding to panel (a). (c) Similar to (a) but estimate is by calculation of initial data to minimize difference between solution and observations. Minimization was carried out on observations from $t = 0$ through $t = 7$ (see arrow). Beyond $t = 7$, the heavy line represents the solution to the Lorenz equations with the calculated initial data.

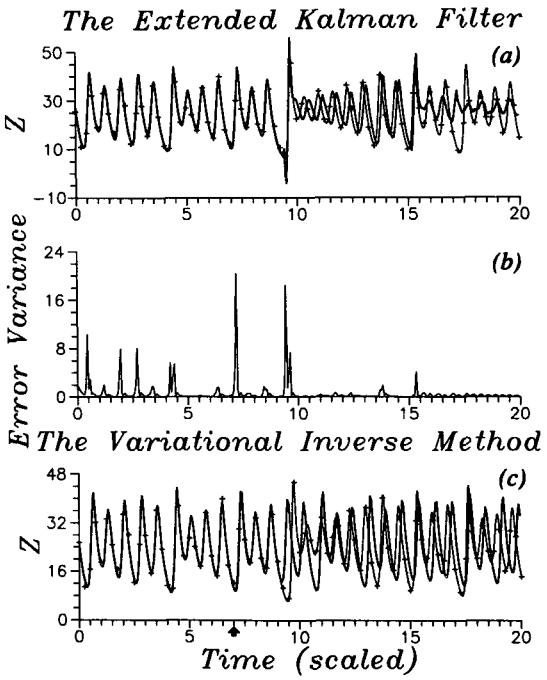

FIG. 4. Similar to Fig. 3 but for Z variable.

near $t = 10$, followed the subsequent transition at $t = 12$ with large phase errors, and underwent a transition near $t = 14$ which the reference solution did not undergo. Near $t = 15$, the true solution passed to the basin of the state with X and Y positive, and remained there for nearly 4 time units. Near $t = 17$, the spike in the estimated error variance (Figs. 3b and 4b) gave rise to a filter correction that forced the solution into the correct basin for one half-loop, but the filter did not track the subsequent transition of the reference system. For the most part, the filter estimate is unreliable beyond $t = 11$.

Figures 4a and 4b show the evolution of the Z variable and the associated estimate of its error variance. From this plot alone, one cannot distinguish which convective basin the estimated and true state vectors are in, but simultaneous examination of Figs. 3 and 4 reveals those times when the states approach the origin, and thus explains the spikes in the variance records. These spikes will occur only in the region of phase space in which trajectories are most unstable. After each correction, the estimated error covariance is always less than the observation error covariance, so the system must be very unstable indeed to produce significant error growth in a single assimilation cycle.

One of the linearized growth rates must always be negative, since the sum of the eigenvalues must be the trace of the linearized system of equations, which is a negative constant (Lorenz 1963). Intuitively, this decaying mode reflects the stability of the attractor itself. Following a perturbation, which takes the state point off the attractor, the state will tend to return to the attractor though not necessarily to the original trajectory. It is this stable mode which is responsible for the apparent stiffness of the evolution equations for the covariance matrix, first noted by E. F. Carter (1990, personal communication). The condition number of the covariance evolution matrix will be the square of that of the state evolution matrix, so for some choices of time step, the covariance calculation will behave badly while the state evolution does not. This difficulty can be overcome through the use of square-root filters (Bierman 1977).

c. Variational methods

It is important to note that the difficulty in tracking a chaotic orbit by assimilating noisy observations results from the inherent instability of the system rather than from that of the data assimilation method. Figures 3c, 4c, and 5 show the results of an inverse calculation. In this calculation, the conjugate gradient method was used to estimate initial data for the solution to the Lorenz system, which passes closest to the observations in the least-squares sense. As noted in the first section, the gradient of the cost function is often calculated by solving an adjoint problem. In this case, with only three state variables, the gradient can be calculated directly, and no adjoint problem need be solved.

The results shown in Figs. 3c, 4c, and 5 were calculated using the IMSL conjugate gradient routine. Solutions could not be obtained when observations at times greater than 7 were included in the least-squares calculation, and even that was difficult to achieve. Even if the conjugate gradient routine is given the exact solution as its first guess, convergence could not be achieved beyond the interval [0, 7]. It may be possible to produce a conjugate gradient code specifically tailored to the Lorenz equations which will extend the optimization period by some small amount—doing the calculation in double precision will also result in marginal improvement—but the end result will be the same.

The gradient of the cost function in the vicinity of the exact solution can be very large, up to $O(10^3)$. A gradient of that magnitude means that a change in the third decimal place in the initial data will produce a unit change in the cost function. The cost function in this calculation is defined as the mean-square error, which implies that near the minimum the cost function will be ~ 2, so a unit change is quite significant.

The arrows in Figs. 3c, 4c, and 5 show the times up to which the optimal solutions were calculated. In all of the cases shown, the curves were extrapolated out to $t = 20$ by using the solution to the inverse problem at $t = T$ as the initial value for subsequent evolution.

Figure 5 shows the results of two inverse calculations: panel (a) shows the optimal solution for the time interval [0, 7]; panel (b) shows a similar calculation

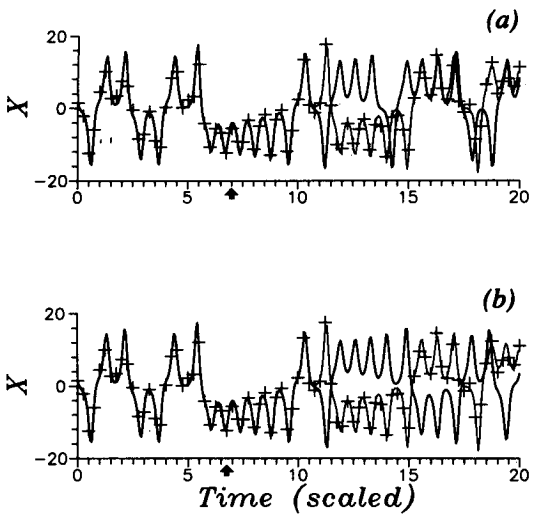

FIG. 5. Sensitivity of the variational method to observations. (a) Calculation of optimal initial values for observations taken over $0 \leq t \leq 7$. Thin line: reference solution; plus signs: simulated observations; heavy line: solution to equations with given initial data. (b) As in panel (a) but for observations over the interval [0, 6.75].

for the time interval [0, 6.75]. The updating interval was 0.25, as noted above, so the two solutions differ only in that the one shown in panel (a) was based on a single observation of the state vector in addition to the one shown in panel (b).

The difficulty of finding the initial values which minimize the least-squares error is illustrated graphically in Fig. 6. This figure shows three examples of graphs of values of the cost function in a fixed direction in the three-dimensional space of initial data. The problem of finding the minimum of the curves in panels (b) and (c) is intractable for any line-search minimization algorithm. The unreliability of approximate derivatives will cause secant methods to fail; even if one were able to implement Newton's method in the search direction, the practical problems resulting from the density of local minima would be insurmountable.

It is clear from Fig. 6 that the number of minima increases as the time interval T over which the minimization is carried out increases. We strongly suspect that, in the limit of increasing T, the graph of the cost function becomes fractal, with distinct minima being associated with distinct sheets of the attractor. Multiple minima have been documented for fair-sized models (e.g., Ghil and Malanotte-Rizzoli 1991, Fig. 28, and discussion thereof). White (1993) has shown rigorously for Burgers's equation that a unique minimum obtains only for sufficiently short time intervals.

Weak-constraint methods such as those discussed in the description of the double-well problem may be more successful, but we anticipate difficulties similar to those encountered in that earlier case. Unlike the stochastically forced double well, the Lorenz model is entirely deterministic, so in order to formulate a weak-constraint method, we would have to devise some procedure for finding reasonable values for the covariances of the model residuals. Such a procedure will be described in the next section.

Direct calculation of the cost-function minimum, with each point in time and phase space considered as an independent variable, is much more cumbersome in this case than in the double-well example, since the number of variables is an order of magnitude larger. Bennett and Thorburn (1991) used a weak-constraint method successfully with a fully nonlinear quasigeostrophic model, but that model did not exhibit the extreme nonlinear behavior observed in the double-well and Lorenz models.

d. Generalizations of the EKF

The earlier failure of the straightforward application of the EKF was attributed to insufficient gain. This could be remedied by more frequent or more accurate observations, as we found in section 3. A condition similar to that obtained for the double-well model probably applies; that is, the gain must be roughly 0.5 in order to force a transition from one state to the other.

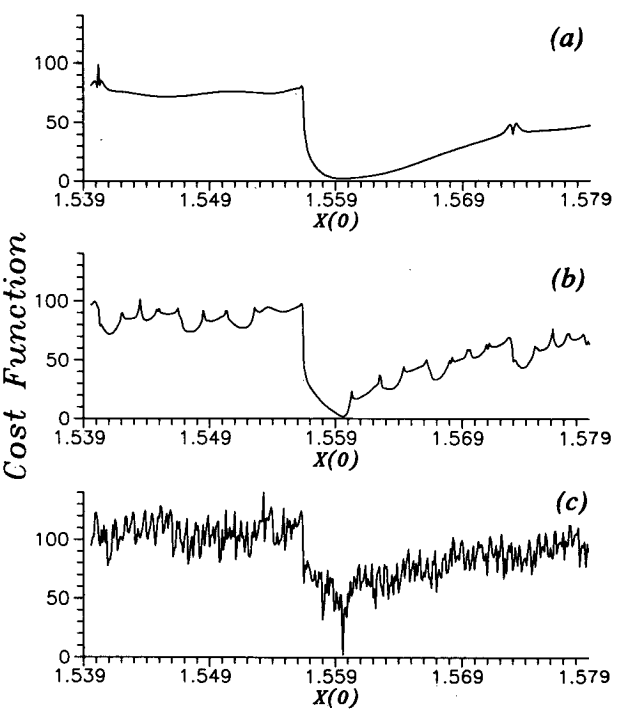

FIG. 6. Values of cost function as a function of initial X, with initial Y and Z held constant, in the neighborhood of the initial values used in calculating the reference solution. (a) Cost function, i.e., mean-square deviation of model solution with given initial data from "observed" values, where observations up to $t = 8$ are considered. (b) As in (a) but for observations up to $t = 10$. (c) As in (a) but for observations up to $t = 15$.

From the gain formula (2.6), this means that the estimated forecast-error variance must be roughly equal to the observation-error variance. As noted above, this will be difficult to obtain within the framework of the standard EKF. We therefore must find some way to augment the estimate of the forecast error covariance, and hence the gain.

1) HIGHER-ORDER EKF

Conceptually, one of the simplest things to do is to estimate the higher moments, which are neglected in the EKF. This technique was used successfully by Kushner (1967) in his study of the Van der Pol oscillator, in which third moments as well as those higher than fourth were in fact neglected. As in the case of Kushner's experiments with the Van der Pol oscillator, calculation of moments up to and including fourth order is sufficient here for the calculation of the evolution of the error covariance.

The covariance matrix in this case was calculated according to the straightforward generalization of (2.3) to vector equations, with moments of fifth order and higher discarded. The forecast values of both the third and fourth moments were calculated in a similar straightforward fashion, consistent with this level of approximation. The forecast value of the third-order moments is defined as

$$\Theta_n^f(i,j,k) = E[(x_{n,i}^t - x_{n,i}^f)(x_{n,j}^t - x_{n,j}^f)(x_{n,k}^t - x_{n,k}^f)],$$

where $x_{n,j}^t$ is the jth component of the true state vector at time step n, and similarly for the components of the forecast state vector $x_{n,j}^f$. The fourth-order moments are defined similarly:

$$\Gamma_n^f(i,j,k,l) = E[(x_{n,i}^t - x_{n,i}^f)(x_{n,j}^t - x_{n,j}^f) \times (x_{n,k}^t - x_{n,k}^f)(x_{n,l}^t - x_{n,l}^f)].$$

An evolution equation for Θ_n^f can be derived analogously to Eq. (2.4) for P:

$$\Theta_n^f(i,j,k) = \sum_{l,m,p} \frac{\partial F_i}{\partial x_l}\frac{\partial F_j}{\partial x_m}\frac{\partial F_k}{\partial x_p}\Theta_{n-1}^a(l,m,p) - \frac{1}{2}\sum_{l,m,p,q}\left[\frac{\partial F_i}{\partial x_l}\frac{\partial F_j}{\partial x_m}\frac{\partial^2 F_k}{\partial x_p \partial x_q} + \frac{\partial F_j}{\partial x_l}\frac{\partial F_k}{\partial x_m}\frac{\partial^2 F_i}{\partial x_p \partial x_q} + \frac{\partial F_k}{\partial x_l}\frac{\partial F_i}{\partial x_m}\frac{\partial^2 F_j}{\partial x_p \partial x_q}\right]\Gamma_{n-1}^a(l,m,p,q), \quad (4.2a)$$

where F_i, F_j, and F_k are the right-hand sides of (4.1a) through (4.1c), respectively, and the partial derivatives are evaluated at the analyzed state variables. The evolution of the fourth moments is calculated similarly and yields

$$\Gamma_n^f(i,j,k,l) = \sum_{p,q,r,s}\frac{\partial F_i}{\partial x_p}\frac{\partial F_j}{\partial x_q}\frac{\partial F_k}{\partial x_r}\frac{\partial F_l}{\partial x_s}\Gamma_{n-1}^a(p,q,r,s), \quad (4.2b)$$

since fifth-order moments are neglected. The updating of Θ and Γ at assimilation times is done consistently with the gain matrix K_n, which is specified in terms of P and R alone, as in the unmodified EKF:

$$\Theta_n^a(i,j,k) = \sum_{l,p,q}(I-K_n)(i,l)(I-K_n)(j,p) \times (I-K_n)(k,q)\Theta_n^f(l,p,q), \quad (4.3a)$$

$$\begin{aligned}\Gamma_n^a(i,j,k,l) &= \sum_{p,q,r,s}(I-K_n)(i,p)(I-K_n)(j,q) \\ &\quad \times (I-K_n)(k,r)(I-K_n)(l,s) \\ &\quad \times \Gamma_n^f(p,q,r,s) + \sum_{p,q,r,s} K_n(i,p) \\ &\quad \times K_n(j,q)K_n(k,r)K_n(l,s) \\ &\quad \times \Gamma_n^o(p,q,r,s) + \sum_{p,q,r,s}(I-K_n)(i,p) \\ &\quad \times (I-K_n)(j,q)K_n(k,r) \\ &\quad \times K_n(l,s)P_n^f(p,q)R(r,s) + \cdots, \end{aligned} \quad (4.3b)$$

where the dots represent the permutations of the pairs (i,p), (j,q), (k,r), and (l,s) in the last summation.

Results of the moment expansion are shown in Figs. 7 and 8. With moments up to fourth order included, the generalized EKF tracks the reference solution accurately by producing enough gain to overcome the tendency of the unmodified filter to drift. This can be seen from the evolution of $\mathbf{P}$, shown in Figs. 7b and 8b. Comparison with Figs. 3b and 4b shows that for the initial ten time units, most of the spikes in 3b and 7b occur at the same times, though the unmodified filter tends to produce smaller amplitudes. The generalized EKF produces a strong double spike near $t = 11$, which is clearly apparent in 7b. The unmodified EKF generates a single weaker spike just before this. The comparison of 4b to 8b is similar at this point—the pair of spikes near $t = 10.5$ is much larger in 8b. This is the time at which the ordinary EKF loses track. The third and fourth moments are quite significant, as shown in Figs. 7c and 7d, at transition or near-transition times.

A detailed analysis based on the Fokker–Planck equation shows that if the third moments do not vanish, then the covariance matrix actually depends on the observations themselves (see Kushner 1967; Jazwinski 1970, chapter 6). In the present case, though, the simplified evolution formulas (4.2, 4.3) were evidently sufficient.

2) STOCHASTIC APPROXIMATION

A computationally simpler remedy to the lack of gain near transition is the use of an empirically derived covariance matrix for the system noise. In this case, the dynamical model is perfect, so we should have $\sigma^2 = 0$ in the notation of (2.4). Rather than computing higher

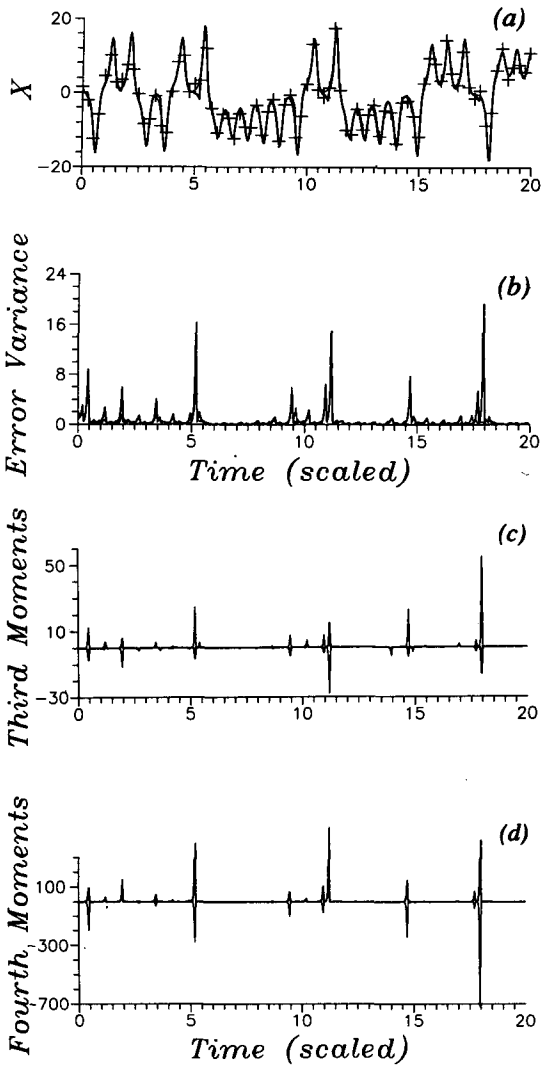

FIG. 7. Results of modified EKF with third- and fourth-order moments calculated explicitly. (a) Estimates of the variable X. Heavy line: filtered solution; thin line: reference solution; "+" signs: simulated observations. (b) Estimated error variances. Heavy line: Estimated error variance for X; thin line: estimated error variance from ordinary EKF. (c) Calculated third error moments. Heavy line: $\Theta(1, 1, 1)$; thin line: $\Theta(1, 3, 3)$. (d) Calculated fourth error moments. Heavy line: $\Gamma(1, 1, 1, 1)$; thin line: $\Gamma(1, 1, 2, 3)$.

moments explicitly, we attempt to account for the higher moments in terms of a constant matrix.

A very simple empirical noise model can be constructed based on the assumption that the right-hand side of (4.1a–c) consists of the sum of the linearized deterministic part and a random forcing term. We can estimate the covariance of the assumed forcing term by a Monte Carlo procedure, and use this to calculate our system-noise covariance. At revision time, we became aware that a similar stochastic error formalism for a similar deterministic model was developed by Nicolis (1992).

In the Monte Carlo experiment, we took 10 000 Gaussian-distributed random initial states, with mean equal to one of the convective states, and covariance equal to $2\mathbf{I}$—where $\mathbf{I}$ is the 3×3 identity matrix—since this is the observation-error covariance. For each of these initial states, we used two models to calculate the evolution of the system for an observing interval $\Delta t = 0.25$. One model was the full nonlinear model (4.1a–c). The other was a linear model with constant coefficients that was constructed by linearizing (4.1a–c) about the appropriate convective state, that is

$$\dot{x} = \sigma(y - x), \tag{4.4a}$$

$$\dot{y} = x - y - x_0 z, \tag{4.4b}$$

$$\dot{z} = Y_0 x + X_0 y - \beta z, \tag{4.4c}$$

where lowercase letters indicate deviation from the critical point (X_0, Y_0, Z_0). We then ran the linear and nonlinear models for an interval $\Delta t = 0.25$. A histogram of the differences between linear and nonlinear runs is shown in Fig. 9.

Even after a time interval of only 0.25, this distribution is clearly non-Gaussian. Furthermore, the variance does not increase linearly, or even monotonically, with time, as would be consistent with the simple model (4.4). Nevertheless, the mean deviation from linearity is not significantly different from zero at the 95% level, and we can calculate the sample covariance $\mathbf{P}_s$.

The evolution of the forecast-error covariance in this case is given by the vector form of Eq. (2.4) for the case of linear dynamics:

$$\mathbf{P}^f_{k+1} = \mathbf{L}\mathbf{P}^a_k\mathbf{L}^{\mathrm{T}} + \mathbf{Q},$$

where $\mathbf{Q}$ is the covariance of the random forcing and $\mathbf{L}$ defines the evolution of the state vector $\mathbf{x}$:

$$\mathbf{x}^f_{k+1} = \mathbf{L}\mathbf{x}^a_k.$$

For fixed $\mathbf{L}$ and $\mathbf{Q}$,

$$\mathbf{P}^f_k = \mathbf{L}^k\mathbf{P}^a_0{\mathbf{L}^k}^{\mathrm{T}} + \sum_{j=0}^{k-1} \mathbf{L}^j\mathbf{Q}(\mathbf{L}^j)^{\mathrm{T}}.$$

We thus wish to choose $\mathbf{Q}$ such that

$$\sum_{j=0}^{k-1} \mathbf{L}^j\mathbf{Q}(\mathbf{L}^{\mathrm{T}})^j = \mathbf{P}_s \tag{4.5}$$

(see also Cohn et al. 1981; Ghil et al. 1981). We may solve conveniently for $\mathbf{Q}$ by writing

$$\mathbf{Q} = \mathbf{U}\mathbf{A}\mathbf{U}^*,$$

where $\mathbf{U}$ is the matrix whose columns are the eigenvectors of $\mathbf{L}$ and the asterisk denotes conjugate transpose. The sum then becomes:

$$\sum_{j=0}^{k-1} \mathbf{L}^j\mathbf{Q}(\mathbf{L}^{\mathrm{T}})^j = \mathbf{U}\Big(\sum_{j=0}^{k-1} \Lambda^j\mathbf{A}(\Lambda^j)^*\Big)\mathbf{U}^*,$$

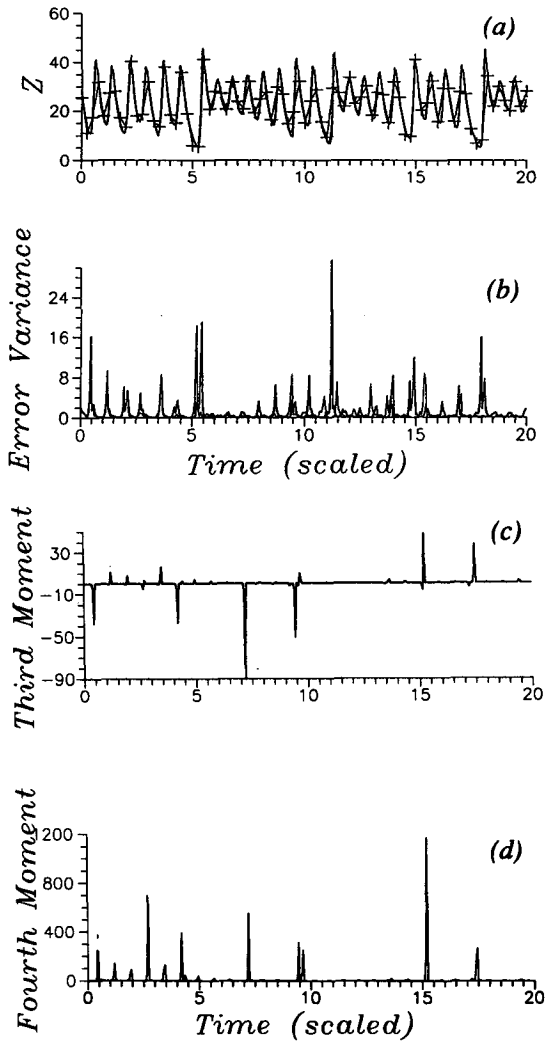

FIG. 8. Results of modified EKF with third- and fourth-order moments calculated explicitly. (a) Estimates of the variable Z. Reference solution and filtered solution are shown. The "+" signs denote simulated observations. (b) Estimated error variances. Heavy line: estimated error variances for Z from the moment expansion calculation; thin line: estimated error variances from unmodified EKF. (c) Third-moment calculation: $\Theta(3, 3, 3)$. (d) Fourth-moment calculation: $\Gamma(3, 3, 3, 3)$.

where $\Lambda = \mathrm{diag}(\lambda_1, \lambda_2, \lambda_3)$ is the diagonal matrix whose nonzero entries are the eigenvalues of $\mathbf{L}$. This can be evaluated by the sum formula for geometric series as follows:

$$\sum_{j=0}^{k-1} [\Lambda^j \mathbf{A} (\Lambda^j)^*]_{lm} = \sum_{j=0}^{k-1} \lambda_l^j \mathbf{A}_{lm} (\lambda_m^j)^* = \mathbf{A}_{lm}[1 - \lambda_l^k (\lambda_m^k)^*]/(1 - \lambda_l \lambda_m^*).$$

Thus, given $\mathbf{P}_s$, we can in theory calculate an appropriate $\mathbf{Q}$. Inversion of the above formula is poorly conditioned in this case, but a reasonable $\mathbf{Q}$, that is, one

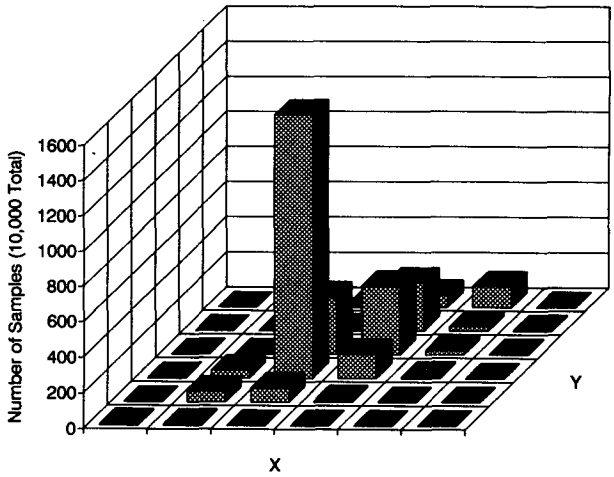

FIG. 9. Results of Monte Carlo simulation. Histogram of deviations from linearity of the Lorenz system in the neighborhood of a convective state. Histogram shown is for those samples whose Z coordinate appeared within 0.2σ of the linearized system. This amounts to roughly 3000 of 10 000 realizations in the experiment. The X and Y bins are 0.4σ wide; the standard deviations σ are sample statistics.

that nearly satisfies (4.5), may be computed by assuming that $\mathbf{A}$ is diagonal.

Results of the application of the modified EKF with this value of $\mathbf{Q}$ are shown in Fig. 10. The graph of the output of the modified filter is extremely close to that of the true solution. The estimated values of $P(1, 1)$ and $P(3, 3)$, the error variances of X and Z, are shown in Figs. 11a and 11b, respectively. Figure 11 is comparable to Figs. 7b and 8b. Hence, this modification achieves very good results at a much smaller computational cost and complexity than the fourth-order EKF.

The empirical $\mathbf{Q}$ obtained by Monte Carlo simulation could be used to construct a weak-constraint var-

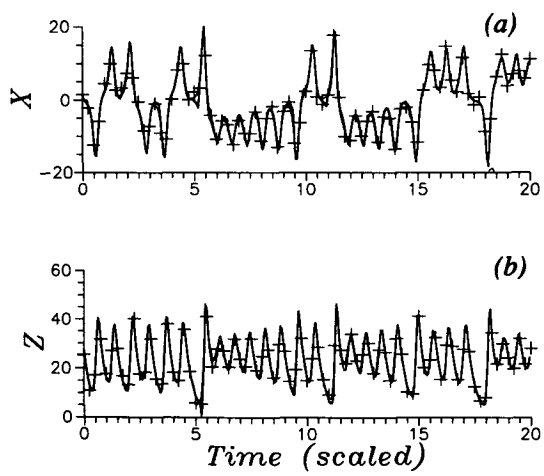

FIG. 10. Results of EKF with empirical noise model. (a) Evolution of X. (b) Evolution of Z. Heavy line: filtered output; thin line: reference solution; "+" signs: simulated observations.

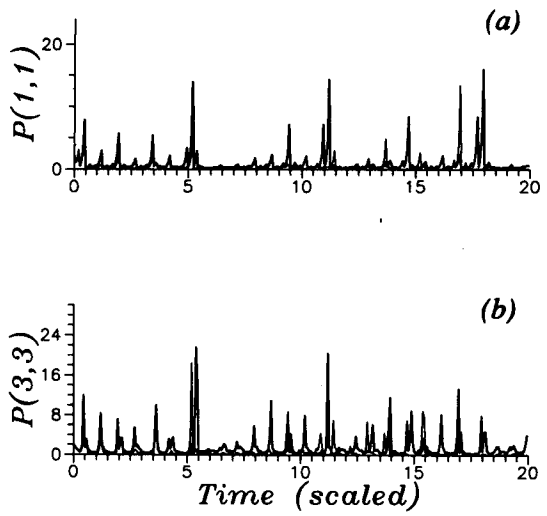

FIG. 11. Estimated error variances with empirical noise model. (a) Estimated error variance $P(1, 1)$ of X. (b) Estimated error variance $P(3, 3)$ of Z. Heavy line: filter with empirical noise model; thin line: unmodified EKF.

iational method. Such a method would produce results at least as good as those shown in Fig. 10, but would suffer from the computational problems described in section 3c.

5. Concluding remarks

A number of studies have addressed the performance of data assimilation methods in the presence of the advective nonlinearities that characterize geophysical flow problems, either in the short term (Budgell 1986; Courtier and Talagrand 1987; Derber 1989) or at equilibrium (Schröter and Wunsch 1986; Tziperman and Thacker 1989). We have concentrated in this study on the performance of advanced assimilation methods for time-dependent problems over longer time intervals, in the combined presence of strong nonlinearity—leading in particular to multimodality—and of vigorous instability—such as might be associated with rapid growth of barotropic and baroclinic disturbances in the atmosphere and oceans. Different methods from sequential estimation—the usual extended Kalman filter (EKF) and three modifications thereof—and from control theory—weak- and strong-constraint variational methods—were applied to two simple models with interesting features: the stochastically perturbed double-well potential and the Lorenz system.

a. The double-well problem

Simple as it may be, the double-well model illustrates clearly certain important problems for data assimilation. In order for the EKF to function adequately for longer times, the observation noise or the observation interval have to be sufficiently small for given system noise (Fig. 1). This is a consequence of the bimodality of the system. A linear system responds proportionately: a less accurate observation is weighted less heavily, and thus exerts less influence on the resulting analysis, while still reducing the estimation error by a modest amount. In the case of bimodality, this proportional response may be insufficient. The observation-error covariance and the forecast-error covariance must combine in such a way as to provide enough gain to force the system over the threshold between the basins of attraction of the two stable equilibria. The desired combination is achieved with relative ease by a simple modification of the EKF, based on examining the innovation sequence (Fig. 2).

We have seen that the strong-constraint approach cannot be applied at all to a model with stochastic uncertainties, and that computational difficulties arise in the weak-constraint approach; these difficulties are also intimately related to the nonlinearity of the system. The Euler–Lagrange equations (3.2) cannot be solved by successive approximations because of the necessity of estimating the large anomalies that are needed to force the system from one stable equilibrium to the other. The quasi-linearization techniques found in the engineering literature are difficult to apply because the nonlinearity defeats the strategy of integrating the adjoint equation backwards separately from the forward integration of the dynamical model itself.

Even when a weak-constraint method is applied by direct minimization, the results are less than satisfactory. Our experience was that application of the variational smoother did result in somewhat smoother solutions, but we were unable to produce a solution to the variational problem that was qualitatively different from the first guess, provided by the modified EKF above.

Similar results on the application of the EKF to the double-well model were obtained by F. LeGland (1991, personal communication). He computed the evolution of the probability density of the solution by integrating the Zakai equation (Rozovskii 1990) given a noisy series of observations. In an example of the double well in which he initialized the system in the wrong basin, he obtained a bimodal distribution that developed larger amplitude in the correct basin as observations accumulated, until, after enough observations had been processed—his observation process was continuous, so this occurs after one relaxation time—one could be, say, 95% confident that the system was in the correct basin. The probability distribution yields all of the information one might desire, but such calculations are overwhelming in scale for realistic atmospheric and ocean models, since the Zakai equation is a parabolic partial differential equation with a number of independent (space) variables equal to the number of components on the state vector in the original problem.

b. The Lorenz model

The Lorenz model, while still very simple, presents the added challenge of the uncertainty arising not from additive stochastic forcing but from the intrinsic instabilities of the deterministic dynamics. In a realistic geophysical flow model, uncertainties arise both from the unstable deterministic interactions between those scales of motion resolved and from the statistical uncertainty in the effect of the unresolved scales on the former. The full consideration of both effects is under investigation and left for a subsequent publication.

In the case of the Lorenz model, both the standard EKF—using only first- and second-order moments—and the strong-constraint variational method fail to follow transitions of the system from one type of motion to another, after a time interval that is a moderate multiple of the characteristic time of the system—the convective overturning time (Figs. 3 and 4). In the atmosphere this corresponds, say, to failure to track transitions between blocked and zonal flow after a few weeks—that is, a moderate multiple of the lifetime of a midlatitude weather system. In the ocean it might correspond to failure to track transitions between the large-meander and small-meander state of the Kuroshio after a few seasons—that is, a similar multiple of the lifetime of rings and eddies in the midlatitude ocean.

Continuous tracking for the EKF can be easily extended by reducing either the observation error (cf. Fig. 1a) or the observing interval (cf. Fig. 1c). In the case of a strong-constraint method, the difficulty is harder to circumvent (Fig. 5), since the cost function exhibits more and more minima as the time interval over which the minimization is performed increases (Figs. 6a–c). Similar results were obtained by Gauthier (1992). One possibility in the latter case is to break up the interval over which the trajectory is fitted to the data into subintervals, which will lead to discontinuities in the solution (cf. Derber 1989). Another one is to introduce explicit error terms into the equations, which is in fact equivalent to the application of a weak-constraint method. Such a method could be most effectively applied by using both the covariance structure and the first guess from a modified EKF, as in the double-well problem (cf. Fig. 2).

Two interesting modifications to the EKF were introduced in section 4, distinct from the one applied in section 3. Calculation of third- and fourth-order moments of the forecast error, along with the customary first- and second-order ones of the EKF, permits near-perfect tracking for an indefinite time (Figs. 7 and 8). Comparison of the behavior of the forecast-error variance for the usual and the modified EKF shows that they are quite small most of the time, and it is only the difference in their values at or near transition that yields the crucial improvement in the latter. Higher-order moment calculation would be impractical, however, for more realistic, highly resolved models of the atmosphere and oceans.

A more efficient and apparently equally successful (Fig. 10) modification of the EKF can be based on using linearization of the governing equations and Monte Carlo simulation to obtain the second moment of the deviation between the trajectories of the linearized and the nonlinear system (Fig. 9). In practice, such linearized versions already exist for a number of operational or quasi-operational numerical weather prediction models, or are relatively easy to construct (e.g., Nigam et al. 1986: Branstator 1990). As Monte Carlo simulation also becomes expensive for large models, it could be replaced, most likely, by calculation of forecast-error covariances from lagged-average forecasts (Kalnay and Dalcher 1987a,b). The estimated trajectory from such a computationally feasible, modified EKF could then be further smoothed if desired, by a weak-constraint method using the covariance structure and the first guess of the EKF.

The results show that the way to tracking rapid instabilities of, and transitions between, geophysical flow regimes passes through advanced data assimilation methods. While they might help point this way, the results also highlight some of the obstacles, and indicate that considerable advances, theoretical and computational, are still necessary to achieve a failproof, realistic data assimilation system capable of handling vigorous instabilities and strong nonlinearities in extended-range prediction.

Acknowledgments. We learned about engineering techniques such as the "sanity checker" from James Thorpe and had useful discussions about variational methods with Olivier Talagrand. François LeGland kindly shared his unpublished results on integration of the Zakai equation. Drs. Eugenia Kalnay, Joseph J. Tribbia, and an anonymous reviewer helped improve the presentation of the results. Ms. Barbara McVicar aided in the preparation of the manuscript. This work was supported by ONR Contract N00014-90-J-1125 and NSF Grant OCE-8800004 (RNM), by NSF Grant OCE-8919439, ONR Grant N00014-90-J-1481, NASA Grant NAG-5713, a Guggenheim Fellowship (MG), and a Fellowship from the Fondation de l'Ecole Polytechnique (FG). MG would like to thank Dr. R. Sadourny and the entire staff of the Laboratoire de Météorologie Dynamique, Ecole Normale Supérieure, Paris, for a pleasant and productive sabbatical.

APPENDIX A

Numerical Considerations for Stochastic Differential Equations

The explicit trapezoidal rule (second-order predictor–corrector), generalized for stochastic differential equations (Klauder and Petersen 1985; Kloeden and Pearson 1977), leads to complications: when linear-

ized, these methods do not generate Langevin-type equations with deterministic drift because the operator itself depends on the random trajectory. The derivation of the extended Kalman filter (EKF) for this case differs slightly from the standard formulation.

We derive here the discrete form of the EKF in the specific case of the use of the explicit trapezoidal rule to calculate the evolution of the system state and the covariance. The true system is assumed to evolve according to the stochastic differential equation (SDE)

$$d\mathbf{x}^t = \mathbf{f}(\mathbf{x}^t)dt + d\mathbf{b}, \tag{A.1}$$

where b is a Wiener process. This is approximated to second order by the two-step scheme:

$$\tilde{\mathbf{x}}^t_{k+1} = \mathbf{x}^t_k + \Delta t\mathbf{f}(\mathbf{x}^t_k) + \sqrt{\Delta t}\tilde{\mathbf{b}}_{k+1}, \tag{A.2a}$$

$$\mathbf{x}^t_{k+1} = \mathbf{x}^t_k + (\Delta t/2)[\mathbf{f}(\mathbf{x}^t_k) + \mathbf{f}(\tilde{\mathbf{x}}^t_{k+1})] + \sqrt{\Delta t}\mathbf{b}_{k+1}, \tag{A.2b}$$

where $E(\tilde{\mathbf{b}}_j\mathbf{b}_k^{\mathrm{T}}) = 0$; $E(\tilde{\mathbf{b}}_j\tilde{\mathbf{b}}_k^{\mathrm{T}}) = E(\mathbf{b}_j\mathbf{b}_j^{\mathrm{T}}) = \mathbf{Q}\delta_{jk}$.

The linearized form of (A.2) is not of the Langevin type, since the partial derivatives of $\mathbf{f}$ evaluated at $\tilde{\mathbf{x}}^t_{k+1}$ depend upon the realization. Implementation of the EKF by this method is therefore a mild generalization of the standard EKF. The forecast-model evolution is given by

$$\tilde{\mathbf{x}}^f_{k+1} = \mathbf{x}^a_k + \Delta t\mathbf{f}(\mathbf{x}^a_k),$$

$$\mathbf{x}^f_{k+1} = \mathbf{x}^a_k + (\Delta t/2)[\mathbf{f}(\mathbf{x}^a_k) + \mathbf{f}(\tilde{\mathbf{x}}^f_{k+1})].$$

The evolution of the error is given by

$$\begin{aligned}\mathbf{x}^t_{k+1} - \mathbf{x}^f_{k+1} \equiv \mathbf{e}^f_{k+1} &\approx \mathbf{e}^a_k + (\Delta t/2)[D\mathbf{F}\mathbf{e}^a_k + \widetilde{D\mathbf{F}}\tilde{\mathbf{e}}^f_{k+1}] \\ &\quad + \sqrt{\Delta t}\mathbf{b}_{k+1} \approx [\mathbf{I} + (\Delta t/2)(D\mathbf{F} + \widetilde{D\mathbf{F}}) \\ &\quad + (\Delta t^2/2)\widetilde{D\mathbf{F}}D\mathbf{F}]\mathbf{e}^a_k \\ &\quad + \Delta t^{1/2}\mathbf{b}_{k+1} + \tfrac{1}{2}\Delta t^{3/2}\widetilde{D\mathbf{F}}\tilde{\mathbf{b}},\end{aligned}$$

where $D\mathbf{F}$ is the Jacobian of $\mathbf{f}$, evaluated at $\mathbf{x}^a_k$, and $\widetilde{D\mathbf{F}}$ the Jacobian of $\mathbf{f}$, evaluated at $\tilde{\mathbf{x}}^f_{k+1}$, with

$$\mathbf{e}^a_k \equiv \mathbf{x}^t_k - \mathbf{x}^a_k, \quad \tilde{\mathbf{e}}^f_{k+1} \equiv \mathbf{x}^t_{k+1} - \tilde{\mathbf{x}}^f_{k+1}.$$

Quadratic and higher-degree expressions in $\mathbf{e}^a_k$ have been neglected.

The evolution of the error covariance is given by

$$\begin{aligned}\mathbf{P}^f_{k+1} = E(\mathbf{e}^f_{k+1}\mathbf{e}^{f\mathrm{T}}_{k+1}) &= \mathbf{M}\mathbf{P}^a_k\mathbf{M}^{\mathrm{T}} \\ &\quad + \tfrac{1}{2}\Delta t^3\widetilde{D\mathbf{F}}Q\widetilde{D\mathbf{F}}^{\mathrm{T}} + \Delta t\mathbf{Q},\end{aligned}$$

where

$$\mathbf{M} = \mathbf{I} + (\Delta t/2)(D\mathbf{F} + \widetilde{D\mathbf{F}}) + (\Delta t^2/2)\widetilde{D\mathbf{F}}D\mathbf{F},$$

$$\begin{aligned}\mathbf{M}\mathbf{P}\mathbf{M}^{\mathrm{T}} &= \mathbf{P} + \frac{\Delta t}{2}(D\mathbf{F} + \widetilde{D\mathbf{F}})\mathbf{P} \\ &\quad + \frac{\Delta t}{2}\mathbf{P}(D\mathbf{F} + \widetilde{D\mathbf{F}})^{\mathrm{T}} \\ &\quad + (\Delta t^2/2)\{D\tilde{\mathbf{F}}D\mathbf{F}\mathbf{P} + \mathbf{P}D\mathbf{F}^{\mathrm{T}}\widetilde{D\mathbf{F}}^{\mathrm{T}} \\ &\quad + \tfrac{1}{2}(D\mathbf{F} + \widetilde{D\mathbf{F}})\mathbf{P}(D\mathbf{F} + \widetilde{D\mathbf{F}})^{\mathrm{T}}\} + \mathrm{O}(\Delta t^3).\end{aligned}$$

We now compare this to the second-order predictor–corrector solution of the continuous equation for the covariance equation, which may be written as

$$\dot{\mathbf{P}} = D\mathbf{F}\mathbf{P} + \mathbf{P}D\mathbf{F}^{\mathrm{T}} + \mathbf{Q}.$$

This is approximated at discrete times by

$$\tilde{\mathbf{P}}^f_{k+1} = \mathbf{P}^a_k + \Delta tD\mathbf{F}\mathbf{P}^a_k + \Delta t\mathbf{P}D\mathbf{F}^{\mathrm{T}},$$

$$\begin{aligned}\mathbf{P}^f_{k+1} = \mathbf{P}^a_k &+ (\Delta t/2) \\ &\times (D\mathbf{F}\mathbf{P}^a_k + \mathbf{P}^a_kD\mathbf{F}^T + D\tilde{\mathbf{F}}\tilde{\mathbf{P}}^f_{k+1} + \tilde{\mathbf{P}}^f_{k+1}D\tilde{\mathbf{F}}),\end{aligned}$$

$$D\tilde{\mathbf{F}}\tilde{\mathbf{P}}^f_{k+1} = \widetilde{D\mathbf{F}}\mathbf{P}^a_k + \Delta tD\tilde{\mathbf{F}}D\mathbf{F}\mathbf{P}^a_k + \Delta t\widetilde{D\mathbf{F}}\mathbf{P}D\mathbf{F}^{\mathrm{T}},$$

$$\tilde{\mathbf{P}}^f_{k+1}D\tilde{\mathbf{F}}^{\mathrm{T}} = \mathbf{P}^a_k\widetilde{D\mathbf{F}}^{\mathrm{T}} + \Delta tD\mathbf{F}\mathbf{P}^a_kD\tilde{\mathbf{F}}^{\mathrm{T}} + \Delta t\mathbf{P}^a_kD\mathbf{F}^{\mathrm{T}}\widetilde{D\mathbf{F}}^{\mathrm{T}}.$$

Finally,

$$\begin{aligned}\mathbf{P}^f_{k+1} &= \mathbf{P}^a_k + (\Delta t/2)(D\mathbf{F} + \widetilde{D\mathbf{F}})\mathbf{P}^a_k \\ &\quad + (\Delta t/2)\mathbf{P}^a_k(D\mathbf{F} + \widetilde{D\mathbf{F}})^{\mathrm{T}} \\ &\quad + (\Delta t^2/2)[\widetilde{D\mathbf{F}}D\mathbf{F}\mathbf{P}^a_k + \widetilde{D\mathbf{F}}\mathbf{P}D\mathbf{F}^{\mathrm{T}} \\ &\quad + D\mathbf{F}\mathbf{P}^a_k\widetilde{D\mathbf{F}}^{\mathrm{T}} + \mathbf{P}^a_kD\mathbf{F}^{\mathrm{T}}\widetilde{D\mathbf{F}}^{\mathrm{T}}] + \Delta t\mathbf{Q} \\ &= \mathbf{M}\mathbf{P}\mathbf{M}^{\mathrm{T}} + \Delta t\mathbf{Q} + \mathrm{O}(\Delta t^3),\end{aligned}$$

since $\|\widetilde{D\mathbf{F}} - D\mathbf{F}\| = \mathrm{O}(\Delta t)$. So the straightforward generalization of the EKF to the predictor–corrector scheme is equivalent to a second-order method for the solution of the continuous evolution equation for the error covariance, accurate to third order in the time increment, with third and higher moments neglected.

APPENDIX B

Bimodality in the Lorenz Model

It might appear surprising at first to discuss probability and statistics for a deterministic system. But in fact the mechanics of throwing a die are perfectly deterministic. It is only that for certain phenomena, typ-

ically those affected by a large number of degrees of freedom, mathematical models have been developed that attempt to evaluate solely certain gross properties of the phenomenon, such as the mean and (co)variances of given quantities.

In the past, the description of irregular behavior, in time and space, has been abandoned to such probabilistic models and termed *random*. We now understand, based on the work of Lorenz (1963), Ruelle and Takens (1971), and Smale (1967), among others, that irregular behavior can also arise from a deterministic interaction of as few as three degrees of freedom, and call such behavior *chaotic*.

Bimodality in the Lorenz model, while not as easily characterized as bimodality in the double well, is quite real and quantifiable by both analytic and statistical methods. It is most obvious in the return maps. Figure B1 shows the intersections in the ascending direction, that is, those with $dZ/dt > 0$, of a long trajectory with the $Z = 27$ plane. Similar figures may be found in Sparrow (1982).

Other views of the bimodality of the solutions of the Lorenz equations can be gained by computing various functionals of the invariant measure preserved by these equations. It has been well known since the end of the last century how to attach a unique probability measure, invariant under the flow, to conservative systems governed by *Hamiltonian dynamics*. The flow in such systems is on (hyper-) surfaces defined by constant energy, and there is one such surface through every (accessible) point in phase space. Liouville's theorem states that the phase-space flow is incompressible, and hence the unique *invariant measure* is simply the volume of a given phase-space element.

Hamiltonian systems are an interesting but very small subset of all possible dynamical systems. In particular, the general class of systems of greatest interest for geophysical fluid flows are *forced dissipative* ones (Lorenz 1963; Ghil and Childress 1987, chapters 5 and 6). In these systems, the flow is not volume preserving, but volume reducing, tending asymptotically to a set of zero volume, the attractor set. Attractors include fixed points (equilibria), limit cycles (periodic solutions), tori (sets of quasi-periodic solutions), and *strange attractors* (Ruelle and Takens 1971).

Defining invariant measures on strange attractors of forced-dissipative systems is considerably more complicated than on the entire phase space of Hamiltonian systems. But an ergodic theory of chaos and strange attractors (e.g., Eckmann and Ruelle 1985) is now well developed. The intuitive concept, which is hard to work out in suitable generality with all mathematical rigor, is that of letting the entire phase space flow onto the attractor to define an essentially unique invariant measure, the Sinai–Ruelle–Bowen (SRB) measure. The existence of such a measure is indispensable for computing meaningfully the fractal dimension of a strange attractor or the Lyapunov exponents of the flow on it

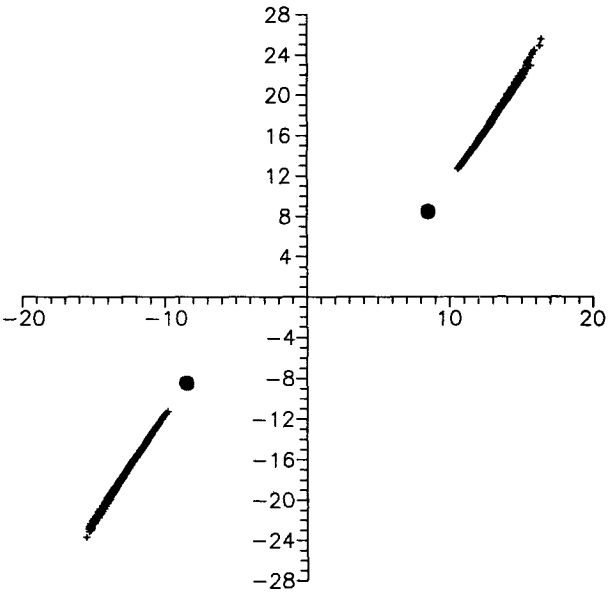

FIG. B1. Poincaré return map for the $Z = 27$ plane for a long integration, from $t = 0$ to $t = 800$, of the Lorenz equations; "+" denotes ascending intersection of the trajectory with the plane. Large filled circles denote the convective states $\pm X = \pm Y = 72^{1/2}$.

(Ghil et al. 1991 and references therein); the latter characterize precisely the divergence of trajectories of interest in this paper.

Mathematical niceties notwithstanding, one of the most obvious things to do for the system (4.1) is to attempt to estimate the density of X or Y. While no rigorous results on the existence or global properties of an SRB measure for the Lorenz model exist, it is generally believed to possess such a measure; a number of its global properties have been determined numerically (Lücke 1976; Knobloch 1979) and some of its local properties, near the unstable manifold of the origin, have been determined by asymptotic methods (Graham and Scholz 1980). We use kernel estimation methods (see Silverman 1986) to estimate the density of the X distribution based on a long integration of the Lorenz equations (4.1). The kernel estimate of the probability density of a univariate process at a point x is given by

$$\hat{f}(x) = \frac{1}{nh} \sum_{j=1}^{n} K[(x - x_j)/h],$$

where K is a judiciously chosen kernel function with the property that $\int_{-\infty}^{\infty} K(y)dy = 1$. We recover the ordinary histogram by choosing $K = 0.5\chi([-1, 1])$, where χ is the characteristic function. Once the kernel is chosen, it is necessary to select an appropriate kernel width h. If the kernel is too wide, then variations in the density function will be smoothed over; if it is too narrow, spurious variation will occur in the estimated distribution function due to discretization.

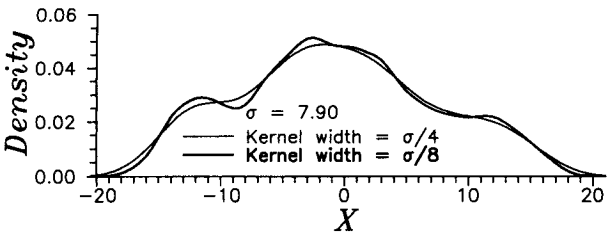

FIG. B2. Density estimate of the variable X for a long integration of the Lorenz equations. The Gaussian kernel, $K(y) = (2\pi)^{-1/2} \times \exp(-y^2/2)$ was used here, with two choices of width indicated on the figures. Similar results were obtained with the biweight and uniform kernels.

A number of different kernels of several different widths were tried, with similar results. An example is shown in Fig. B2. As the kernel width narrows, the structure of the distribution exhibits a large peak near zero (one can show analytically that $\hat{X} = 0$; e.g., Knobloch 1979), and two other peaks near ± 12.5. This is the distribution one would expect from a sample made up of oscillations about two critical points, the picture presented in section 4a. It is easy to verify that the histogram obtained by sampling a normalized harmonic oscillation has symmetrical peaks at ± 1.

Statistical methods for detecting changes in the mean of a stochastic process can be applied successfully to sampled solutions of the Lorenz equations. One method for testing the hypothesis of a shift in the mean of a stochastic process is the sequential Mann–Kendall statistic. This nonparametric test was used by Maasch (1988) to detect the mid-Pleistocene transition in isotopic data from deep sea cores.

For the series $X_{i=1,\cdots,N}$ obtained from a long integration of the Lorenz equations, we calculate for each X_i the value m_i, the number of preceding values that were smaller than X_i. We then calculate the value $d_n = \sum_{i=1}^{n} m_i$ for $1 \leq n \leq N$. Mann (1945) showed that for a stationary time series d_n is normally distributed for large n, with $E(d_n) = n(n-1)/4$ and $\text{var}(d_n) = n(n-1)(2n+5)/72$. To test the statistical significance of d_n, we calculate the Mann–Kendall rank statistic $U(d_n) = [d_n - E(d_n)]/[\text{var}(d_n)]^{1/2}$. A null hypothesis of no change in the underlying mean is rejected for large values of this statistic.

Despite the nonparametric nature of the Mann–Kendall statistic, application of this test to the Lorenz model requires some care. If the individual oscillations with period ≈ 1 are well resolved by the sampling process, the Mann–Kendall statistic will reveal significant trend, as it would in any well-resolved oscillatory process. To eliminate this effect, one may subsample the series itself, or examine the series of residuals calculated by linearizing the equations about the nearest equilibrium point and using the resulting linear initial value problem to predict the next value in the series. Figure B3 shows an example of detection of a transition in the series X_i taken from the extension of the run used to generate the results given in section 3. We use the Mann–Kendall rank statistic for the retrograde series $U'(d_i) = -U(d_{i'})$, where $i' = n + 1 - i$, together with the forward statistic $U(d_i)$ to localize the transition. The two Mann–Kendall statistics taken together localize the transition close to its point of visual occurrence. Similar results are obtained for all other visually observed transitions.

One could use the Mann–Kendall statistic to construct yet another version of the "sanity checker" described in section 3c. Appropriate formulations for analysis and prediction in geophysical fluid dynamics may be hard to come by due to the essentially univariate nature of the test.

From the Mann–Kendall test and from the estimation of the probability density, we see that statistical tools verify our general picture of the qualitative behavior of the Lorenz equations. Other statistical tools, such as the signal-to-noise ratio (Maasch 1988), would most likely yield similar results, given appropriate sample size and sampling rate.

Similar methods were applied by Ghil (1987) and by Kimoto and Ghil (1993a,b) to large-scale atmo-

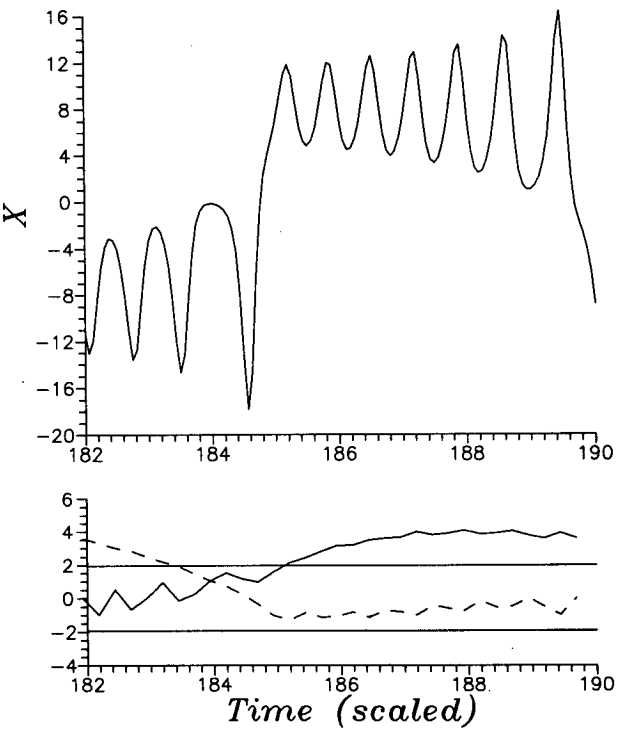

FIG. B3. Detection of a transition with the sequential Mann–Kendall statistic. The upper frame shows a transition taken from the long integration used to construct Figs. B1 and B2. The lower frame shows the forward (solid curve) and retrograde (dashed curve) sequential Mann–Kendall statistics for the sequence shown in the upper frame, subsampled at intervals of 0.25. The horizontal lines define the 95% confidence interval for rejection of the null hypothesis.

spheric flows. Multiple flow regimes, more subtle than the originally contemplated bimodality between zonal and blocked flow in Northern Hemisphere midlatitudes (Charney and deVore 1979; Dole and Gordon 1983), were identified and described synoptically. Tracking of impending transitions between such regimes (Vautard et al. 1990) could benefit from the methodology described here, especially since the estimates of transition times generated by the Mann–Kendall statistic appear slightly ahead of their visual occurrence (cf. Figure B3).

REFERENCES

Bennett A. F., and W. P. Budgell, 1989: The Kalman smoother for a linear quasi-geostrophic model of ocean circulation. *Dyn. Atmos. Oceans,* **13,** 219–267.

——, and M. A. Thorburn, 1991: The generalized inverse of a nonlinear quasi-geostrophic ocean circulation model. *J. Phys. Oceanogr.,* **22,** 213–230.

Bierman, G. J., 1977: *Factorization Methods for Discrete Sequential Estimation.* Academic Press, 241 pp.

Branstator, G., 1990: Low-frequency patterns induced by stationary waves. *J. Atmos. Sci.,* **47,** 629–648.

Bryson, A. E., and Y-C Ho, 1975: *Applied Optimal Control.* Hemisphere Publishing, 481 pp.

Budgell, W. P., 1986: Nonlinear data assimilation for shallow water equations in branched channels. *J. Geophys. Res.,* **91,** 10 633–10 644.

Chao, S-Y, 1984: Biomodality of the Kuroshio. *J. Phys. Oceanogr.,* **14,** 92–103.

Charney, J. G., and J. G. DeVore, 1979: Multiple flow equilibria in the atmosphere and blocking. *J. Atmos. Sci.,* **36,** 1205–1216.

Cohn, S. E., M. Ghil, and E. Isaacson, 1981: Optimal interpolation and the Kalman filter. *Fifth Conf. on Numerical Weather Prediction,* Amer. Meteor. Soc., 36–42.

Constantin, P., C. Foias, B. Nicolaenko, and R. Témam, 1989: *Integral Manifolds and Intertial Manifolds for Dissipative Partial Differential Equations.* Springer-Verlag, 121 pp.

Courant, R., and D. Hilbert, 1953: *Methods of Mathematical Physics,* Vol. 1. Wiley-Interscience, 560 pp.

Courtier, P., and O. Talagrand, 1987: Variational assimilation of meteorological observations with the adjoint vorticity equation. II: Numerical results. *Quart. J. Roy. Meteor. Soc.,* **113,** 1329–1347.

Derber, J. C., 1989: A variational continuous assimilation technique. *Mon. Wea. Rev.,* **117,** 2437–2446.

Dole, R. M., and N. D. Gordon, 1983: Persistent anomalies of the extratropical Northern Hemisphere wintertime circulation: Geographical distribution and regional persistance characteristics. *Mon. Wea. Rev.,* **111,** 1567–1586.

Eckmann, J. P., and D. Ruelle, 1985: Ergodic theory of chaos and strange attractors. *Rev. Mod. Phys.,* **57,** 617–656.

Forsythe, G. E., and C. B. Moler, 1967: *Computer Solution of Linear Algebraic Systems.* Prentice-Hall, 148 pp.

Gaspar, P., and C. Wunsch, 1989: Estimates from altimeter data of barotropic Rossby waves in the northwestern Atlantic Ocean. *J. Phys. Oceanogr.,* **19,** 1821–1844.

Gauthier, P., 1992: Chaos and quadri-dimensional data assimilation: A study based on the Lorenz model. *Tellus,* **44A,** 2–17.

Gelb, A., Ed., 1974: *Applied Optimal Estimation.* The MIT Press, 374 pp.

Ghil, M., 1987: Dynamics, statistics and predictability of planetary flow regimes. *Irreversible Phenomena and Dynamical Systems Analysis in the Geosciences,* C. Nicolis and G. Nicolis, Eds., D. Reidel, 241–283.

——, 1989: Meteorological data assimilation for oceanographers. Part I: Description and theoretical framework. *Dyn. Atmos. Oceans,* **13,** 171–218.

——, and S. Childress, 1987: *Topics in Geophysical Fluid Dynamics: Atmospheric Dynamics, Dynamo Theory and Climate Dynamics.* Springer-Verlag, 485 pp.

——, and P. Malanotte-Rizzoli, 1991: Data assimilation in meteorology and oceanography. *Advances in Geophysics,* Vol. 33, Academic Press, 141–266.

——, S. E. Cohn, J. Tavantzis, K. Bube, and E. Isaacson, 1981: Applications of estimation theory to numerical weather prediction. *Dynamic Meteorology: Data Assimilation Methods,* L. Bengtsson, M. Ghil and E. Källén, Eds., Springer-Verlag, 139–224.

——, ——, and A. Dalcher, 1982: Sequential estimation, data assimilation, and initialization. *The Interaction between Objective Analysis and Initialization,* D. Williamson, Ed., Publ. Meteorol. 127, Proc. 14th Stanstead Seminar, McGill University, Montreal, pp. 83–97.

——, M. Kimoto, and J. D. Neelin, 1991: Nonlinear dynamics and predictability in the Atmospheric Sciences. *Rev. Geophys.,* **36**(Suppl.), 46–55.

Graham, R., and H. J. Scholz, 1980: Analytic approximation of the Lorenz attractor by invariant manifolds. *Phys. Rev. A,* **22,** 1198–1204.

Guckenheimer, J., and P. Holmes, 1983: *Nonlinear Oscillations, Dynamical Systems, and Bifurcations of Vector Fields.* Springer-Verlag, 453 pp.

IMSL Math/Library, Version 1.1, 1989: *FORTRAN Subroutines for Mathematical Applications.* IMSL Inc., 2500 Park West Tower One, 2500 City West Boulevard, Houston, TX, 77042–3020.

Jazwinski, A. H., 1970: *Stochastic Processes and Filtering Theory.* Academic Press, 376 pp.

Kailath, T., 1968: An innovations approach to least-squares estimation. Part I: Linear filtering in additive white noise. *IEEE Trans. Automat. Contr.,* **AC-13,** 646–655.

Kalnay, E., and A. Dalcher, 1987a: Forecasting forcast skill. *Mon. Wea. Rev.,* **115,** 349–356.

——, and ——, 1987b: Error growth and predictability in operational ECMWF forecasts. *Tellus,* **39A,** 479–491.

Kimoto, M., and M. Ghil, 1993a: Multiple flow regimes in the Northern Hemisphere winter. Part I: Methodology and hemispheric regimes. *J. Atmos. Sci.,* **50,** 2625–2643.

——, and ——, 1993b: Mulitple flow regimes in the Northern Hemisphere winter. Part II: Sectorial regimes and preferred transitions. *J. Atmos. Sci.,* **50,** 2645–2673.

Klauder, J. R., and W. P. Petersen, 1985: Numerical integration of multiplicative-noise stochastic differential equations. *SIAM J. Numer. Anal.,* **22,** 1153–1166.

Kloeden, P. E., and R. A. Pearson, 1977: The numerical solution of stochastic differential equations. *J. Austral. Math. Soc.,* Ser. B, **20,** 8–12.

Knobloch, E., 1979: On the statistical dynamics of the Lorenz model. *J. Stat. Phys.,* **20,** 695–709.

Kramers, H. A., 1940: Brownian motion in a field of force and the diffusion model of chemical reactions. *Physica,* **7,** 284–304.

Kushner, H., 1967: Approximation to optimal nonlinear filters. *IEEE Trans. Autom. Control,* **AC-12,** 546–556.

Lacarra, J. F., and O. Talagrand, 1988: Short-range evolution of small perturbations in a barotropic model. *Tellus,* **40A,** 81–95.

Le Dimet, F. X., and O. Talagrand, 1986: Variational algorithms for analysis and assimilation of meteorological observations: Theoretical aspects. *Tellus,* **38A,** 97–110.

Legras, B., and M. Ghil, 1985: Persistent anomalies, blocking and variations in atmospheric predictability. *J. Atmos. Sci.,* **42,** 433–471.

Libchaber, A., 1985: The onset of weak turbulence: An experimental introduction. M. Ghil, R. Benzi, and G. Parisi, Eds., *Turbulence and Predictability in Geophysical Fluid Dynamics and Climate Dynamics.* North-Holland, 18–28.

Lorenz, E. N., 1963: Deterministic non-periodic flow. *J. Atmos. Sci.,* **20,** 130–141.

Lücke, M., 1976: Statistical dynamics of the Lorenz model. *J. Stat. Phys.,* **15,** 455–475.

Maasch, K., 1988: Statistical detection of the mid-Pleistocene transition. *Clim. Dyn.*, **2,** 133–143.

Mann, H. B., 1945: Non-parametric test against trend. *Econometrika,* **13,** 245–259.

Masuda, A., 1982: An interpretation of the bimodal character of the stable Kuroshio path. *Deep-Sea Res.*, **29,** 471–484.

May, R., 1973: *Stability and Diversity in Model Ecosystems.* Princeton University Press, 235 pp.

Miller, R. N., and M. Ghil, 1990: Data assimilation in strongly nonlinear current systems. *Proc. Int. Symp. on Observations in Oceanography and Meteorology.* Clermont-Ferrand, France, World Meteorological Organization, 93–98.

Nicolis, C., 1992: Probabilistic aspects of error growth in atmospheric dynamics. *Quart. J. Roy. Meteor. Soc.*, **118,** 553–567.

——, and G. Nicolis, 1981: Stochastic aspects of climatic transitions—additive fluctuations. *Tellus,* **33,** 225–234.

Nigam, S., I. M. Held, and S. W. Lyons, 1986: Linear simulation of stationary eddies in a general circulation model. Part I: The no-mountain model. *J. Atmos. Sci.,* **43,** 2944–2961.

Provost, C., and R. Salmon, 1986: A variational method for inverting hydrographic data. *J. Mar. Res.*, **44,** 1–34.

Rinzel, J., and R. N. Miller, 1980: Numerical calculation of stable and unstable periodic solutions to the Hodgkin–Huxley equations. *Math. Biosci.* **49,** 27–59.

Rozovskii, B. L., 1990: *Stochastic Evolution Systems: Linear Theory and Application to Nonlinear Filtering.* Kluwer Academic, 315 pp.

Ruelle, D., and F. Takens, 1971: On the nature of turbulence. *Commun. Math. Phys.*, **20,** 167–192.

Sasaki, Y., 1958: An objective analysis based on the variational method. *J. Meteor. Soc. Japan,* **36,** 77–88.

——, 1970: Some basic formalisms in numerical variational analysis. *Mon. Wea. Rev.*, **98,** 875–883.

Schröter, J., and C. Wunsch, 1986: Solution of nonlinear finite difference ocean models by optimization methods with sensitivity and observational strategy analysis. *J. Phys. Oceanogr.*, **16,** 1855–1874.

Schuss, Z., 1980: *Theory and Applications of Stochastic Differential Equations.* J. Wiley, 321 pp.

Silverman, B. W., 1986: *Density Estimation for Statistics and Data Analysis.* Chapman and Hall, 175 pp.

Smale, S., 1967: Differential dynamical systems. *Bull. Amer. Math. Soc.*, **73,** 747–817.

Sparrow, C., 1982: *The Lorenz Equations: Bifurcations, Chaos and Strange Attractors.* Springer-Verlag, 269 pp.

Sutera, A., 1980: Stochastic perturbation of a pure convective motion. *J. Atmos. Sci.*, **37,** 245–249.

——, 1981: On stochastic perturbations and long-term climate behavior. *Quart. J. Roy. Meteor. Soc.*, **107,** 137–152.

Témam, R., 1988: *Infinite-Dimensional Dynamical Systems in Mechanics and Physics.* Springer-Verlag, 500 pp.

Thacker, W. C., and R. B. Long, 1988: Fitting dynamics to data. *J. Geophys. Res.*, **93,** 1227–1240.

Tziperman, E., and W. C. Thacker, 1989: An optimal-control/adjoint-equations approach to studying the oceanic general circulation. *J. Phys. Oceanogr.*, **19,** 1821–1844.

Vautard, R., K.-C. Mo, and M. Ghil,' 1990: Statistical significance test for transition matrices of atmospheric Markov chains. *J. Atmos. Sci.*, **47,** 1926–1931.

White, L. W., 1993: A study of uniqueness for the initialization problem for Burger's equation. *J. Math. Anal. Appl.*, **172,** 412–431.